Remote Sensing of Environment 216 (2018) 697–714

Contents lists available at ScienceDirect

Remote Sensing of Environment

journal homepage: www.elsevier.com/locate/rse

Three decades of forest structural dynamics over Canada's forested ecosystems using Landsat time-series and lidar plots

Giona Matasci[a], Txomin Hermosilla[a], Michael A. Wulder[b], Joanne C. White[b], Nicholas C. Coops[a,*], Geordie W. Hobart[b], Douglas K. Bolton[a], Piotr Tompalski[a], Christopher W. Bater[c]

[a] Integrated Remote Sensing Studio, Department of Forest Resources Management, University of British Columbia, 2424 Main Mall, Vancouver, BC V6T 1Z4, Canada
[b] Canadian Forest Service, Pacific Forestry Centre, Natural Resources Canada, 506 West Burnside Road, Victoria, BC V8Z 1M5, Canada
[c] Forest Management Branch, Forestry Division, Alberta Agriculture and Forestry, Edmonton, Alberta T5K 2M4, Canada

ARTICLE INFO

Keywords:
Landsat
Lidar
Forest recovery
Imputation
Canopy cover
Biomass

ABSTRACT

Attributes that describe forest structure, such as height, canopy cover, volume, and biomass, are required to inform forest inventories and monitoring programs. Light Detection and Ranging (lidar) has been successfully demonstrated as a means to derive a suite of forest structure attributes at the plot level; however, these acquisitions are often constrained to limited spatial extents and to a given point in time. Sample based approaches for model development can accommodate the spatial limitations of lidar acquisitions when characterizing large areas. The combination of lidar plot data and time-series satellite imagery is well suited to provide spatially extensive, and temporally dense, information on forest structure and related dynamics over very large areas. In this research, we combine lidar plot-derived information with Landsat pixel-based composites to produce annual forest structure estimates from 1984 to 2016 over 650 million ha of Canada's forest ecosystems using a nearest neighbor imputation approach with a Random Forests-based distance metric. Imputed variables included lidar metrics of height (e.g., mean height, standard deviation of height) and cover, as well as area-based modelled inventory estimates of Lorey's height, basal area, stem volume, and biomass. Models were validated using reserved validation plots, with model R^2 ranging from 0.62 to 0.64 for lidar metrics of height and cover, and R^2 of 0.67, 0.68, 0.71, and 0.70 for Lorey's height, basal area, volume and biomass, respectively. Unique to this study was the assessment of model extension through time, with model performance for imputing lidar metrics evaluated at the forest stand-level using independent lidar data representing a latitudinal gradient of forest conditions and that was not used in model development. The period evaluated was 2006–2012, with R^2 values ranging from 0.36 to 0.66 for height metrics, and 0.47–0.77 for cover metrics. Ultimately, we show how deriving forest structural estimates on an annual basis enables the analysis of both the dynamics and regional trends of undisturbed forest, as well as regenerating stands following stand-replacing disturbances (i.e., fire, harvesting).

1. Introduction

Monitoring plays a foundational role in supporting sustainable forest management, and informing the development of policies aimed at preserving and maintaining ecosystem services and biodiversity in forests while concurrently accommodating human needs (Daily, 1997). Moreover, spatially-explicit estimates of forest attributes inform reporting activities by providing data for forest (White et al., 2014) and carbon (Boisvenue et al., 2016) monitoring programs. National forest inventory programs are typically designed to produce long-term data in support of forest monitoring (Kangas and Maltamo, 2006; MacDicken, 2015). Many of these programs, however, are sample-based and aspatial, and cannot provide spatially-explicit inputs for modelling unless they are combined with other forms of inventory data or remotely sensed data (e.g., Beaudoin et al., 2014; Tomppo et al., 2009). Thus, there is a need for spatially-explicit forest monitoring information collected at a resolution suitable for capturing anthropogenic impacts, and supporting a range of scientific and policy elements. Furthermore, the capacity to generate this information retrospectively can provide useful baseline information for understanding forest dynamics (White et al., 2017) and for modelling potential vulnerabilities to climate change (Price et al., 2013). In addition, a time-series of forest structure

* Corresponding author.
E-mail address: nicholas.coops@ubc.ca (N.C. Coops).

https://doi.org/10.1016/j.rse.2018.07.024
Received 9 May 2018; Received in revised form 17 July 2018; Accepted 21 July 2018

Table 1
Forest structural variables estimated in this study. Lidar returns elevation values are normalized to the ground surface.

Nature of variables	Forest structural variable	Variable name	Units	Description
Extracted directly from point cloud	Mean canopy height	elev_mean	m	Mean height of lidar first returns
	Standard deviation of canopy height	elev_sd	m	Standard deviation of first returns height
	Coefficient of variation of canopy height	elev_cv	–	Coefficient of variation of first returns height
	95th percentile of canopy height	elev_p95	m	95th percentile of first returns height
	Canopy cover	cover_2m	%	Percentage of first returns above 2 m
	Canopy cover above mean height	cover_mean	%	Percentage of first returns above the mean height
Modelled inventory attributes	Lorey's mean height	loreys_height	m	Average height of trees weighted by their basal area
	Basal area	basal_area	m^2/ ha	Cross-sectional area of tree stems at breast height. The sum of the cross-sectional area (i.e., basal area) of each tree in square metres in a plot, divided by the area of the plot.
	Gross stem volume	stem_volume	m^3/ ha	Individual tree gross volumes are calculated using species-specific allometric equations. Gross total volume per hectare is calculated by summing the gross total volume of all trees and dividing by the area of the plot.
	Total aboveground biomass	ag_biomass	t/ha	Individual tree total aboveground biomass is calculated using species-specific equations. Aboveground biomass per hectare is calculated by summing the values of all trees within a plot and dividing by the area of the plot. Aboveground biomass may be separated into various biomass components (e.g., stem, bark, branches, foliage).

attributes including height, canopy cover, volume, and biomass, can also inform on relative trends in forest growth and condition, as well as post-disturbance forest recovery (Bartels et al., 2016; Frolking et al., 2009; Masek et al., 2011). Further, such a time-series recording forest structure can fill critical information gaps for unmanaged forests, where there exists a paucity of spatially exhaustive forest inventory information (Gillis et al., 2005).

Satellite programs with medium spatial resolution (10–100 m) sensors (Belward and Skøien, 2014), such as those of the Landsat mission, provide data for capturing and characterizing both status and change over terrestrial ecosystems at human scales (Wulder et al., 2008b). Image acquisitions from Landsat sensors including Thematic Mapper (TM), Enhanced Thematic Mapper Plus (ETM+), and Operational Land Imager (OLI) have the spatial grain (30 m spatial resolution), spectral bands (visible to short-wave infrared), and revisit time (single sensor, 16 days) required to study vegetation trends with an annual/seasonal frequency (Kovalskyy and Roy, 2013). Since the launch of Landsat-7 in 1999, Landsat has effectively had an 8-day revisit based upon having two satellites in orbit at any given time. The opening of the multi-decadal Landsat archive (Woodcock et al., 2008), combined with the systematic production of science-supported, analysis-ready data products (e.g., surface reflectance, Vermote et al., 2016) has accelerated a number of methodological developments that have advanced satellite-based monitoring activities (Hansen and Loveland, 2012; Wulder et al., 2012a). The process of using analysis ready data, high performance computing, and robust automated algorithms to characterize large areas over time is reviewed in Wulder et al. (2018).

Previously, image compositing methods were more commonly applied to coarse spatial resolution data sources (Cihlar, 2000; Holben, 1986), which were freely available and had a frequent revisit rate. Free and open access to analysis-ready data led to the application of image compositing approaches to Landsat data (Roy et al., 2010). Image compositing allows clear observations for a given pixel to be selectively used from otherwise cloudy images, resulting in the generation of seasonal or annual, gap-free, composites (Griffiths et al., 2013; Hermosilla et al., 2015a; White et al., 2014). These best-available pixel (BAP) composites (White et al., 2014) result in a data space where the spectral bands can be considered representative of a given point in time (e.g., year, season). Furthermore, using surface reflectance derived from a radiometrically calibrated image data source (Markham and Helder, 2012) results in pixel-level values for a given land cover or forest structural condition that can be considered as temporally invariant (Fekety et al., 2014), enabling the application of models through time and space (Song et al., 2001). Thus, Landsat data have enabled the generation of wall-to-wall estimates of forest structure based on the temporal analysis of the spectral trends and/or the change information provided by Landsat time series data (Bolton et al., 2018; Matasci et al., 2018; Pflugmacher et al., 2014, 2012), and to extend these estimates through time (Deo et al., 2017).

Nearest neighbor (NN) imputation is a demonstrated methodological framework to relate environmental-based predictors and inventory-related attributes (Eskelson et al., 2009; Ohmann and Gregory, 2002), as well as Landsat data and lidar-derived attributes (Zald et al., 2014). With a 1-NN structure, imputation has the advantage of assigning a set of measured attributes that actually occur in a forest stand (at a given donor plot location), ensuring prediction of realistic canopy conditions (Hudak et al., 2008). Imputation has been the primary methodological building block of prior studies that investigated single-year forest structure mapping (Tomppo et al., 2009; Zald et al., 2016). A number of studies have shown promising results in extending imputation models to predict forest structure through time, demonstrating the opportunities offered by the generated outputs to inform the study of forest growth and post-disturbance recovery (Deo et al., 2017; Fekety et al., 2014).

In previous work, we applied an imputation approach using lidar plots and Landsat data and generated spatially explicit, wall-to-wall estimates of ten key forest structural attributes (see Table 1) across Canada's boreal forest for a single year (2010) (Matasci et al., 2018). In this current study, we extend the large-area forest attribute imputation model presented in Matasci et al. (2018) through both time (1984–2016) and space (integrating data from the hemi-boreal zone, see Fig. 1), thereby generating annual estimates of the same set of lidar-based metrics and forest structural attributes for the entire treed extent of Canada's forested ecosystems over 33 years. Our objectives were three-fold: (i) to demonstrate the temporal and spatial extension of the imputation model using a time-series of annual surface reflectance image composites and samples of airborne lidar; (ii) to demonstrate the robustness of the outputs by validating the resulting forest structural estimates using a decade of independent lidar data acquisitions across a latitudinal range of forest conditions; and (iii) to highlight the potential for scientific insights related to growth and recovery over large areas, which are enabled through the use of the time-series of forest structure developed herein.

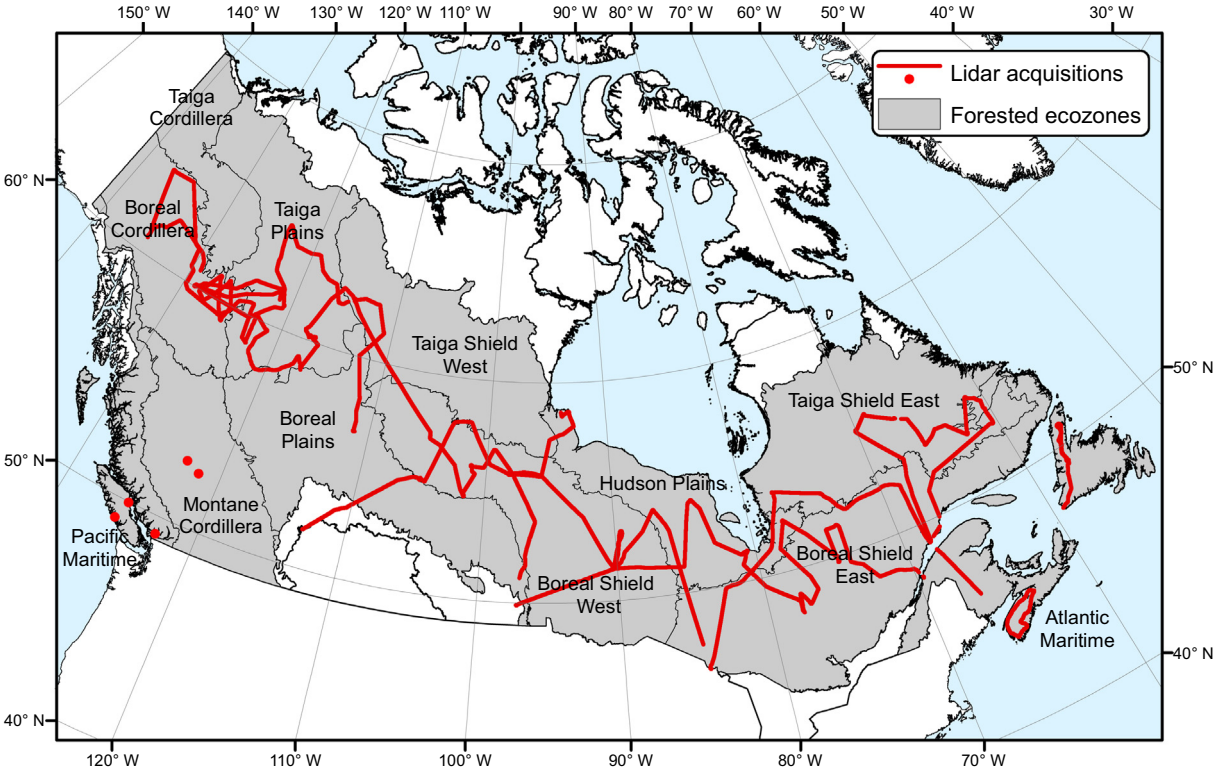

Fig. 1. Canada's forested ecozones and locations of the airborne lidar acquisitions used for model development.

2. Study area

Canada's forest-dominated ecosystems comprise ~650 million ha (65% of the country's total area) (Wulder et al., 2008a). Within these ecosystems, treed areas and other wooded lands occupy 347.1 million ha (Natural Resources Canada, 2016) with the remaining area dominated by lakes and wetlands. While insects represent the primary natural disturbance agent in Canada's forests (by area) (Natural Resources Canada, 2017), wildfires are the primary stand-replacing disturbance, impacting an estimated 40.6 million ha between 1985 and 2010, compared to the 16.7 million ha that were harvested over that same 25-year period (White et al., 2017). Canada's forested ecosystems are partitioned into broad ecozones on the basis of both biotic and abiotic factors, and represent a range of forest abundance and productivity (Fig. 1; Ecological Stratification Working Group, 1996). As the Boreal Shield and Taiga Shield ecozones have large longitudinal extents and consequently a broad range of ecoclimatic conditions from west to east, these ecozones are typically partitioned into a western and eastern component (Frazier et al., 2015; Stocks et al., 2002). While most of forested ecozones are part of the boreal zone, the Montane Cordillera and Pacific Maritime belong to the hemi-boreal zone, which represents the transition between temperate zone and boreal zones.

3. Methods

The methodological framework presented herein enables the temporal extension of a large-area imputation model developed using lidar-derived forest structure measurements and Landsat image composites (Fig. 2). Initially, we computed a set of ten forest structural attributes (Table 1) for lidar plots located across Canada's forested ecosystems (Wulder et al., 2012b). These attributes were our response variables, which we related to a series of co-located and concurrent predictor variables. The main source of these predictor variables was a time-series of Landsat image composites (Hermosilla et al., 2016). Additional predictor variables were the spatial coordinates (latitude and longitude) and terrain features derived from elevation data. A k-NN imputation model was then trained with these data, and applied to all Canada's forested ecozones with predictors values computed for each year in the 1984–2016 sequence, resulting in 33 annual estimates of each of the ten lidar-based metrics and forest structural attributes (or 330 national maps at 30 m resolution). To build confidence in the generated attributes, we validated the lidar metrics using (i) a reserved national set of lidar plots, and (ii) an independent set of multi-temporal regional lidar acquisitions.

3.1. Data

3.1.1. Lidar data

Estimates of forest structure were derived from seven airborne lidar collection campaigns (Table 1). The primary dataset consisted of a national campaign conducted in summer 2010 (34 transects and a total length of 25,000 km; Wulder et al., 2012b). Based upon survey intent, these transects primarily represent boreal forest conditions. As a result, to better represent national forest conditions we augmented these data with six additional lidar datasets representing hemi-boreal conditions (Brandt, 2009). These lidar data were compiled from compatible campaigns conducted in British Columbia (BC), Canada, from 2004 to 2010.

Forest structural attributes characterizing the vertical distribution of vegetation above ground surface (Næsset, 1997) were computed by applying an area-based approach (ABA) within 25 × 25 m cells (Næsset, 2002) using the FUSION software package (McGaughey, 2013). The 25 × 25 m cells were treated as lidar plots during subsequent analysis. In total, the boreal-wide transect comprised > 32 million lidar plots and BC lidar acquisitions involved > 700,000 lidar plots (Table 2). Only those lidar plots identified as treed from the annual land cover map (Hermosilla et al., 2018) were included in the analysis. Six of the ten forest structure metrics (see definitions and units in Table 1) were calculated directly from the lidar point cloud (first returns), including: mean height (elev_mean), standard deviation of height (elev_sd), coefficient of variation of height (elev_cv), 95th

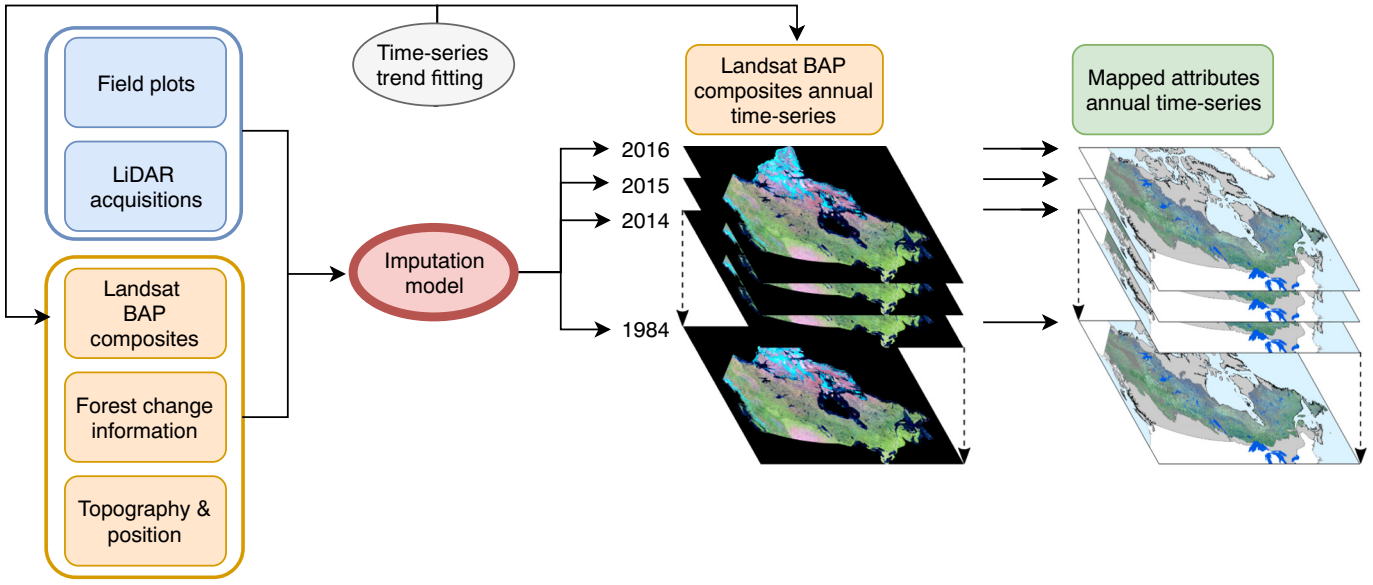

Fig. 2. Workflow for the modelling and mapping of the forest attributes over Canada's forested ecosystems for 1984–2016.

Table 2
Characteristics of lidar acquisitions used to define the imputation models across Canada's forested ecosystems.

Location	Year	Pulse density [pts/m^2]	Reference
Boreal zone	2010	2.8	Wulder et al. (2012b)
Tofino, BC	2005	2.2	Bater et al. (2009)
Alex Fraser Research Forest, BC	2008	2.3	Coops et al. (2010)
Malcolm Knapp Research Forest, BC	2010	3.1	Lu et al. (2015)
Campbell River, BC	2004	3.3	Coops et al. (2007)
Campbell River, BC	2008	4.6	Tompalski et al. (2015)
Quesnel, BC	2008	3.5	Varhola et al. (2010)

percentile of height (elev_p95), canopy cover above 2 m (cover_2m), and canopy cover above cell mean height (cover_mean). Note that heights are normalized to the ground surface. The other four forest structural attributes were modelled inventory attributes derived from the lidar metrics using parametric linear regression and a sample of ground reference plots (Bater et al., 2011; Wulder et al., 2012b), and included: Lorey's mean height (loreys_height), basal area (basal_area), gross stem volume (stem_volume), and total aboveground biomass (ag_biomass). For this task, data from a set of 338 plots (area of 400 m^2) distributed nationally with coincident lidar data and field measurements was compiled (boreal, Bater et al., 2011; Wulder et al., 2012b; hemi-boreal, Bolton et al., 2018, plus as assembled for this research, Table 2). From the plot data, biomass components and gross stem volume were derived from height and diameter at breast height following published equations (Lambert et al., 2005; Marshall and Lemay, 2006; Ung et al., 2008). Following an ABA, the forest attributes were modelled based on the co-located ground reference and lidar metrics, allowing for the application of the models to the nationally distributed lidar data.

As an early adopter of lidar technology and related information for natural resource management, the provincial government of Alberta, Canada, has acquired a near wall-to-wall coverage of lidar data over managed forested lands covering 34 million ha. The current lidar coverage for Alberta represents a patchwork of data acquisition projects, spanning 2003 to 2015, with > 70% of the area acquired between 2006 and 2008. Point densities range between 1 and 4 pulses per m^2 with first return density very consistent and ranging between 0.5 and 0.7 pulses per m^2. Four selected point cloud metrics were derived from these data following similar processing routines (Coops et al., 2016) as those used for the 2010 lidar transects described above (Wulder et al., 2012b): mean height of lidar first returns, 95th percentile of first returns height, percentage of first returns above 2 m, and percentage of first returns above the mean height. Lidar data for the 2006–2012 period were used to derive the yearly reference values for the independent temporal validation.

3.1.2. Landsat data

The predictor variables consisted of a time-series of annual Landsat BAP composites for the period 1984–2016 (after Hermosilla et al., 2015a) and a related forest disturbance history layer (Hermosilla et al., 2015b) generated following the Composite-to-Change (C2C) approach (Hermosilla et al., 2016). A BAP compositing technique (White et al., 2014) utilizing Landsat 5 TM, Landsat 7 ETM+ and Landsat 8 OLI images (Hermosilla et al., 2017) from the United States Geological Survey (USGS) archive was implemented. The criteria to select the *best* pixel for a location and year included proximity to a target date (August 1st, i.e., Julian day 213), distance to clouds and cloud shadows, atmospheric quality, and acquisition sensor (to reduce the impact of Landsat 7 ETM+ acquisitions after the scan line corrector failure). BAP composites were further processed with a spectral trend analysis on pixels' time-series to remove noisy pixels (due to unscreened clouds or shadows) and to fill data gaps (i.e., pixels with no valid observations) (Hermosilla et al., 2015a). We fitted temporal trends to each of the pixel series (Hermosilla et al., 2016, 2015a) to reduce the residual noise in temporal trajectories that can negatively impact the temporal modelling of continuous variables (Pflugmacher et al., 2012). These fitted trends were computed through piecewise linear interpolation between the temporal breakpoints detected (i.e., abrupt changes in Normalized Burn Ratio (NBR) magnitude). This process resulted in a set of seamless, 30 m spatial resolution, annual, surface-reflectance composites that are

radiometrically and phenologically consistent. Additionally the C2C approach allowed the detection and characterization of forest changes, as well as the attribution of these changes into a disturbance type (i.e., fire, harvesting) (Hermosilla et al., 2015b).

Treed areas for each year were identified using the annual land-cover maps of Canada produced using the classification framework presented in Hermosilla et al. (2018), which comprise 12 land-cover classes, including non-vegetated (water, snow/ice, rock/rubble, exposed/barren land), vegetated non-treed (bryoids, herbs, wetland, shrubs), and vegetated treed (wetland-treed, coniferous, broadleaf, mixedwood) (see Wulder et al., 2008a). These annual land-cover maps were generated using a Random Forests (RF) classification (Breiman, 2001) based on the Landsat BAP composites, spectral indices, and elevation derivatives. In order to produce time-consistent maps with ecologically coherent land-cover class transitions, a Hidden Markov Model was applied to incorporate disturbance information and year-to-year vegetation succession expectations (Abercrombie and Friedl, 2016; Gómez et al., 2016; Wulder et al., 2018).

3.1.3. Digital elevation model

The Advanced Spaceborne Thermal Emission and Reflection Radiometer (ASTER) digital elevation model (GDEM V2) was used to generate terrain related predictors that are known to influence forest structure: elevation, slope, topographic wetness index (Beven and Kirkby, 1979), and topographic solar radiation index (Roberts and Cooper, 1989). GDEM V2 was derived using a new production algorithm and 260,000 additional stereo-pairs from the ASTER instrument onboard the Terra satellite, and improves upon the initial GDEM version (computed in 2009) in terms of spatial resolution (effective spatial resolution of 70 m, oversampled to 30 m) and coverage, artifact reduction, and horizontal and vertical accuracies (Tachikawa et al., 2011).

3.2. Sample selection

Samples for model training and validation were selected minimizing spatial autocorrelation, following the approach presented in Matasci et al. (2018) and Zald et al. (2016). Lidar plots were sub-sampled using a hexagonal lattice selecting plots separated by a 250 m spacing. Plots were examined based on a 3 × 3 neighborhood to ensure all nine cells (i) were treed (based on the land cover maps described above), (ii) experienced the same disturbance history (Hermosilla et al., 2015b), and (iii) had moderate canopy height variability (coefficient of variation for elev_p95 < 50% across the nine cells). To avoid the inclusion of non-vegetation outliers, we removed plots with elev_p95 values > 60 or 120 m for the 2010 lidar transect and BC lidar acquisitions, respectively. Finally, we removed plots at the edge of the transect's acquisition swath to avoid high scan angle effects. This preliminary screening resulted in 84,482 lidar plots, from which we randomly selected 75% (63,348) as training samples, and the remaining 25% (21,134) were used as validation samples. Table 3 reports the total number of samples in each ecozone for both training and validation sets.

3.3. Predictor variables

We extracted spatially co-located and temporally concurrent measurements to the lidar plots from the Landsat BAP composites, forest change products, and digital elevation model (see full description in Matasci et al., 2018), including: Tasseled cap brightness (TCB), greenness (TCG), wetness (TCW) and angle (TCA) (Crist, 1985), NBR (Key and Benson, 2006), years since greatest change, elevation, slope, topographic wetness index, topographic solar radiation index, longitude, and latitude.

Table 3
Training and validation plots by ecozone.

Ecozone	Training samples	Validation samples
Atlantic Maritime	2894	950
Boreal Cordillera	11,552	3853
Boreal Plains	2233	754
Boreal Shield East	13,418	4453
Boreal Shield West	12,069	4035
Hudson Plains	3797	1264
Montane Cordillera	650	218
Pacific Maritime	2193	734
Taiga Plains	7125	2372
Taiga Shield East	5499	1868
Taiga Shield West	1918	633

3.4. Imputation approach

To relate predictor and response variables, we followed the same imputation approach applied in Matasci et al. (2018) for single-year mapping (2010) in the boreal zone. By using a NN imputation approach (number of neighbors k = 1), the model seeks the single most representative plot whose values are to be imputed at a given location. The search criterion is based on a non-Euclidean similarity measure computed across all the response variables after having built a series of RF models, one for each of the response variables. This similarity measure is computed as the proportion of trees where the sample to be mapped shares the leaf of the grown forest with a given training sample (Crookston and Finley, 2008; Liaw and Wiener, 2002). The training sample identifier is assigned to the mapping location and its response variable values are retrieved and attributed all at once. The preservation of both the covariance among the response variables and the range of values found in the training data has led to both science and operational uptake of imputation in forestry (Gleason and Im, 2012; Latifi et al., 2010).

The RF-based imputation model was trained on the six lidar metrics (see Section 3.1.1 and Table 1): elev_mean, elev_sd, elev_cv, elev_p95, cover_2m and cover_mean. Corresponding derived forest attributes (loreys_height, basal_area, stem_volume, ag_biomass) associated to the training plots were then imputed to each mapped sample (Matasci et al., 2018; Zald et al., 2016). Algorithm implementation was conducted using the R packages *yaImpute* (Crookston and Finley, 2008) and *randomForest* (Liaw and Wiener, 2002). For continuity with Matasci et al. (2018) and to keep computational time within practical limits, RF parameters were set as follows: *mtry* = 3, *ntree* = 100.

3.5. Model assessment

Two assessment approaches were followed to evaluate the accuracy of our models. First, we applied a national-level assessment of the models using the reserved validation set of lidar plots (n = 21,134 samples; Table 3) across Canada's forested ecosystem according to the reference year, with reference year varying by lidar acquisition date used to inform the model (i.e., 2004, 2005, 2008 or 2010). Second, a novel contribution of this research is a multi-temporal assessment of model performance to demonstrate the quality of the model estimates using the independent lidar data acquired in Alberta. This model assessment at the forest stand level was undertaken using lidar data collected between 2006 and 2012. Forest stands were defined by segmenting Landsat surface reflectance values using eCognition, applying the segmentation parameters proposed by Wulder and Seemann (2003) (scale = 10, colour = 0.7, shape = 0.3, smoothness = 0.5, and compactness = 0.5), which resulted in a total of 6,602,786 objects throughout the seven years. From these objects, the average observed and predicted forest structure attributes were then compared according

to year of lidar acquisition. For both assessment approaches, the following goodness of fit measures for each response variable were computed: coefficient of determination (R^2), root mean squared error (RMSE), RMSE as a percentage of the observed mean (RMSE%), and bias (i.e., average of predicted minus observed values).

3.6. Characterization of forest structure dynamics in Canada's forested-ecosystems

From the national maps produced, we summarized and analyzed dynamics of selected forest attributes (see below) for three scenarios (1984–2016): undisturbed forests, forests impacted by wildfires, and forests impacted by harvesting. Trends and dynamics in stand structure and canopy cover for these three scenarios were characterized by randomly selecting representative pixels based on the forest change type (i.e., undisturbed, fire, and, harvest; Hermosilla et al., 2015b), and examining their full temporal series of predicted forest structure attributes.

Undisturbed pixel samples were selected from areas that did not experience change events between 1984 and 2016, and that were consistently labelled as treed across the analysis period. Significance on trends in undisturbed forested areas was determined by applying non-parametric Mann-Kendall tests (Kendall, 1955; Mann, 1945) on the time-series of annual median values of the distribution of canopy height (elev_p95) and canopy cover (cover_2m). For disturbance events, we analyze these same two lidar-derived metrics as well as two forest attributes: Lorey's height (loreys_height) and total aboveground biomass (ag_biomass). Two strategies were followed to meaningfully depict post-disturbance regrowth. First, to ensure we exclusively capture stand-replacing events (avoiding residual treed patches) we examined the temporal sequence of land-cover labels (Hermosilla et al., 2018) and selected sample pixels that were labelled as treed before the change, and were classified as non-treed for at least three years post-disturbance event. Second, due to the rate of the regrowth in boreal and hemi-boreal forests (Bartels et al., 2016), only a limited number of pixels were classified as treed (condition for our model to assign the set of predicted attributes) following a disturbance event. This resulted in a very small sample that displayed a high variability in the attribute values. To avoid any issues related to small sample size, we modelled growth in the first 10 years following a disturbance using an approach similar to Kurz et al. (2009). This was achieved by fitting a polynomial function (degree 2) for each one of the 25th, 50th and 75th percentile values using an attribute-specific starting point and the respective series of values from 11 to 20 years after disturbance. These starting points were set as follows: 2 m for elev_p95, 5% for cover_2m, 3.5 m for loreys_height or 2 t/ha for ag_biomass. Table 4 reports the number of randomly sampled pixels in each ecozone per change type (i.e., undisturbed, fire, and harvest) used to produce the figures.

Table 4
Number of samples per ecozone by type of change used to develop the forest structure dynamic figures.

Ecozone	Undisturbed	Wildfire	Harvest
Atlantic Maritime	32,267	–	62,863
Boreal Cordillera	232,505	28,507	–
Boreal Plains	175,718	51,781	112,281
Boreal Shield East	316,599	78,093	139,156
Boreal Shield West	163,275	85,364	68,618
Hudson Plains	32,124	12,071	–
Montane Cordillera	80,652	22,202	27,572
Pacific Maritime	60,004	–	60,932
Taiga Cordillera	33,168	3974	–
Taiga Plains	159,532	56,982	12,407
Taiga Shield East	56,990	3752	–
Taiga Shield West	152,328	49,381	–

4. Results

4.1. Model assessment using reserved validation lidar plots

The national assessment results of the imputation models against the validation samples across Canada's forested ecosystem are shown in Table 5. Coefficient of determination R^2 is > 0.61 for all attributes except for those describing height variability (elev_sd, elev_cv). For variables related to stand height, i.e., mean height of lidar first returns (elev_mean), 95th percentile of first returns height (elev_p95) and mean height of trees weighted by their basal area (loreys_height), we observe RMSE values of 2.66 m, 3.77 m and 2.88 m, respectively. In terms of canopy cover metrics, the percentage of first returns above 2 m (cover_2m) and the percentage of first returns above the mean height (cover_mean) have an RMSE of 18.4% and 10.5%. Among the derived forest attributes, we observe an RMSE of 7.38 m^2/ha for basal area (basal_area), 95.54 m^3/ha for gross stem volume (stem_volume) and 41.43 t/ha for total aboveground biomass (ag_biomass). The measure allowing standardized cross-comparisons, the RMSE%, shows values ranging from 24.5 to 82.3%, with lower values for stand height-related variables and higher ones for complex forest attributes such as stem volume and aboveground biomass. In terms of bias, we observe values close to zero across all the response variables, indicating that no major over- or under-estimation in the forest structure prediction.

4.2. Multi-temporal model assessment at the stand level using independent lidar acquisitions

Results of the assessment using the independent lidar data acquisitions for 2006–2012 in Alberta, Canada, are shown in Table 6. Annually the RMSE and RMSE% are generally stable, while the coefficient of determination (R^2) values show larger variability through time. Bias was both positive and negative for individual years, and was consistently larger than bias reported using the reserved validation samples (Table 5). Overall (i.e., when combining all years 2006–2012), the performance of the model, as captured by R^2 and RMSE, was lower for variables related to stand height (elev_mean, elev_p95) and similar for metrics describing canopy cover (cover_2m and cover_mean), relative to assessment results achieved when using the reserved validation plots. Similarly, RMSE% values are comparable for the mean height of lidar first returns (elev_mean) and the 95th percentile of first returns height (elev_p95), and smaller for percentage of first returns above 2 m (cover_2m) and percentage of first returns above the mean height (cover_mean).

4.3. Annual forest structure maps

We produced annual maps from 1984 to 2016 covering Canada's forested ecosystems for the ten imputed forest structure attributes (Table 1) with a spatial resolution of 30 m. The temporal examination of these outputs permits a detailed wall-to-wall analysis of the evolution of forest structure dynamics. As an example, Fig. 3 shows the difference between 2016 and 1984 of the forest structure attributes canopy cover (cover_2m, Fig. 3a), canopy height (elev_p95, Fig. 3b), total aboveground biomass (ag_biomass, Fig. 3c), and Lorey's height (loreys_height, Fig. 3d). Further nuances on forest structure dynamics can be derived from the temporal analysis of undisturbed (Fig. 4) and disturbed (Figs. 5–8) trends.

4.4. Characterization of forest structure dynamics in Canada's forested ecosystems from 1984 to 2016

4.4.1. Undisturbed forest

Fig. 4 shows the annual distribution of canopy height (elev_p95) and canopy cover (cover_2m) attributes from 1984 to 2016 for undisturbed forests, by forested ecozone. The canopy height shows statistically

Table 5
Summary statistics for the observed and predicted lidar metrics and forest attributes with associated accuracy metrics on the 21,134 validation plots. For the description of the variables refer to Table 1.

Resp. variable	Units	Observed				Predicted				Accuracy metrics			
		Mean	Min	Max	Std. dev.	Mean	Min	Max	Std. dev.	R^2	RMSE	RMSE%	Bias
elev_mean	m	6.9	2.11	49.12	4.22	6.86	2.13	46.5	4.17	0.639	2.66	38.6	−0.03
elev_sd	m	2.49	0.06	54.17	1.49	2.47	0.11	18.29	1.44	0.45	1.19	47.8	−0.02
elev_cv	–	0.37	0.03	4.37	0.1	0.37	0.02	0.98	0.1	0.125	0.11	29.7	0
elev_p95	m	11.1	2.22	64.7	5.9	11.03	2.25	58.64	5.84	0.631	3.77	34.0	−0.06
cover_2m	%	44.19	0.27	100	29.07	44.02	0.34	100	29.2	0.642	18.37	41.6	−0.17
cover_mean	%	21.58	0.1	71.47	15.9	21.52	0.1	70.62	15.97	0.616	10.46	48.5	−0.06
loreys_height	m	11.74	3.72	51.29	4.78	11.7	3.76	47.56	4.73	0.666	2.88	24.5	−0.05
basal_area	m^2/ha	15.15	0.87	116.09	12.54	15.04	0.96	117.66	12.43	0.681	7.38	48.7	−0.12
stem_volume	m^3/ha	116.05	1.67	2352.61	172.38	114.54	2.05	2352.61	169.36	0.712	95.54	82.3	−1.51
ag_biomass	t/ha	62.95	1.92	904.02	72.84	62.29	2.17	904.02	71.8	0.699	41.43	65.8	−0.66

Table 6
Multi-temporal accuracy assessment at the stand level using the independent lidar acquisitions. For the description of variables refer to Table 1.

Year	elev_mean [m]				elev_p95 [m]				cover_2m [%]				cover_mean [%]			
	R^2	RMSE	RMSE%	bias	R^2	RMSE	RMSE%	bias	R^2	RMSE	RMSE%	bias	R^2	RMSE	RMSE%	bias
2006	0.38	4.1	38.3	0.44	0.36	5.7	35.1	0.87	0.47	18.6	26.4	1.62	0.47	11.3	30.2	−0.44
2007	0.50	4.1	41.2	0.47	0.47	5.7	36.5	0.67	0.59	18.4	27.3	3.17	0.57	11.4	32.4	1.14
2008	0.53	4.1	40.9	−0.17	0.50	5.5	34.8	−0.55	0.62	18.0	25.5	1.29	0.62	11.1	30.4	0.25
2009	0.50	4.3	43.7	−0.59	0.48	5.7	37.3	−0.99	0.57	18.7	26.8	−1.53	0.58	11.7	31.9	−1.87
2010	0.66	3.5	41.3	0.74	0.65	4.9	34.6	0.17	0.60	18.0	27.2	−0.15	0.63	10.8	32.2	0.39
2011	0.61	3.9	46.6	0.22	0.55	5.4	41.0	0.03	0.69	16.7	26.8	2.35	0.70	10.4	32.3	1.32
2012	0.64	4.4	44.5	−0.01	0.61	5.7	36.8	−0.24	0.77	13.2	18.2	−0.18	0.76	9.0	23.7	−0.81
2006–2012	0.54	4.1	41.4	0.16	0.51	5.50	35.7	−0.01	0.60	17.9	26.0	1.23	0.61	11.1	30.9	0.18

significant positive trends for all ecozones (p-value = 0.000 for Mann-Kendall test on the time-series of median values). Similar significant positive trends were found for canopy cover in all but two ecozones: Montane Cordillera (Mann-Kendall test Z = −6.70), Pacific Maritime (Mann-Kendall test Z = −4.59). Increases in height were greatest in the Boreal Plains, Boreal Shield West, Hudson Plains, and Taiga Plains ecozones, with median height increments between 2 and 3 m over the 33-year period considered.

The magnitude of the imputed values is markedly larger in the ecozones located in the hemi-boreal region (i.e., Montane Cordillera and Pacific Maritime), with median canopy height values of approximately 20 m. On the contrary, the lowest canopy height values are found in Taiga Shield West and Taiga Cordillera, with annual median values lower than 10 m. As would be expected, canopy cover was relatively stable in undisturbed forest over the time period. Atlantic Maritime and Pacific Maritime had the highest canopy cover which remained highly consistent over the time period. The more alpine and mountainous Taiga Cordillera had the lowest cover. While most ecozones had consistent cover associated with undisturbed forests, a number showed annual variations. For instance, the Atlantic Maritime, Taiga Plains and Boreal Plains showed a reduction in variance in canopy cover in these undisturbed stands over the time period.

4.4.2. Post-disturbance dynamics

The annual values of forest structure attributes after wildfire across the ten fire-dominated ecozones (White et al., 2017) are shown in Fig. 5 for metrics extracted directly from the point clouds (cover_2m and elev_p95), and in Fig. 6 for modelled inventory attributes (loreys_height and ag_biomass). Canopy cover increases rapidly following fire disturbances indicating a quick regrowth of the canopy-filling gaps in the horizontal plane. In the most productive ecozones (e.g., Boreal Shield East), canopy cover increased by 40–50% in two decades, reaching pre-fire levels within the analysis period. Canopy height and Lorey's height increased at lower rates in the initial years following fire. Some of the ecozones exhibited a large variability in the imputed values in the final years of the time-series (pattern especially visible for the ag_biomass attribute). This is caused by a smaller sample size as there are a limited number of fire pixel trajectories that are longer than 25 years (i.e., only change events that occurred at the beginning of the observation period).

The annual values of forest structure metrics following harvest across the ecozones where harvest activities are dominant (White et al., 2017) are shown in Fig. 7 for lidar metrics (cover_2m and eleve_p95) and in Fig. 8 for derived forest attributes (loreys_height and ag_biomass). Comparing areas that were harvested to burned areas, on average, pre-disturbance canopy height (elev_p95) is 4 m larger, Lorey's height (loreys_height) is 2 m larger, and total aboveground biomass (ag_biomass) is 30 t/ha larger, since harvest activities generally occur on more productive sites compared to wildfires, which take place in a more diverse set of forest conditions. Similar to wildfires, canopy cover (cover_2m) returns more rapidly to pre-disturbance value than canopy height (elev_p95) and Lorey's height (loreys_height). In terms of vegetation regrowth, in most ecozones we observe a gradual linear response of canopy height and canopy cover when compared to the evolution after fire events. Fig. 9 shows an example of the spatial patterns of forest structure dynamics for the total aboveground biomass (ag_biomass) attribute in a landscape dominated by harvest activities in western Alberta.

5. Discussion

In this paper we present a workflow that enables spatially and temporally complete predictions of six lidar vegetation metrics and four forest inventory attributes at a 30 m spatial resolution, resulting in a multi-decadal, wall-to-wall mapping of 33 years of Canada's forest structure. This research fuses two complementary data sources: a time-series of Landsat surface-reflectance image composites covering Canada for 1984–2016, and airborne lidar plots that extensively sampled Canada's forested ecosystems. Combining these two remotely sensed data sources allows the accurate vertical detail provided by lidar and

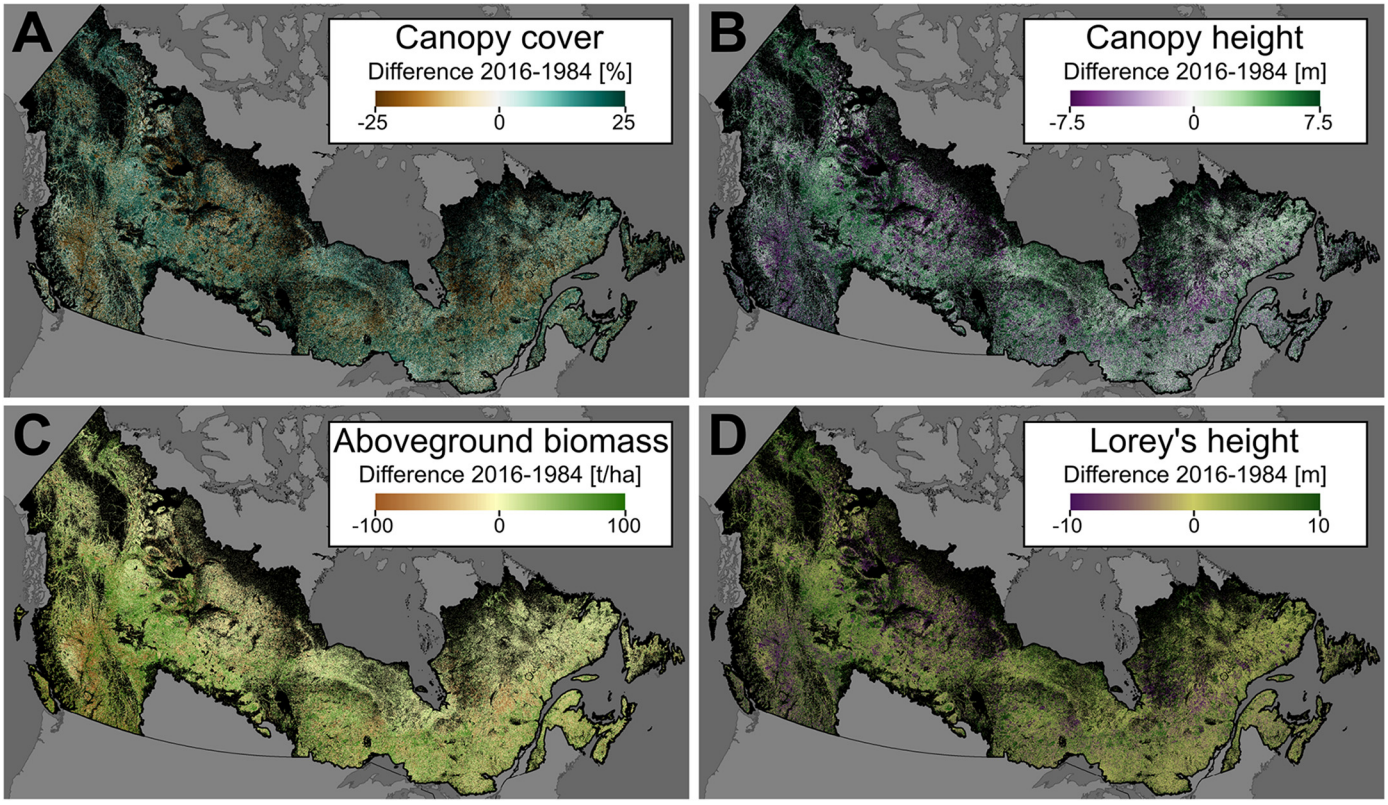

Fig. 3. Difference (2016–1984) maps of forest structure attributes (a) canopy cover (cover_2m), (b) canopy height (elev_p95), (c) total aboveground biomass (ag_biomass), and (d) Lorey's height (loreys_height). Note that values above/below the upper/lower limits are truncated.

the extensive spatial and deep temporal coverage of Landsat imagery to be fully exploited. Through the use of lidar, a spatially distributed source of forest structural attributes for model calibration and validation is possible (Wulder et al., 2012c). Forest structure attributes derived from lidar acquisitions offer high-quality calibration data to develop statistical models based on Landsat time-series (e.g., Bolton et al., 2018, 2015; Zald et al., 2016). Parametric methods such as multiple linear regression or non-parametric options such as RF support the estimation of forest structural attributes to characterize both current conditions (Ahmed et al., 2015; Frazier et al., 2014; Pflugmacher et al., 2012) and historic conditions (Deo et al., 2017; Fekety et al., 2014; Pflugmacher et al., 2014). Multi-temporal predictions of forest attributes based on time-series of Landsat data are typically undertaken using fitted trends on spectral values (e.g., polynomial curves, piecewise linear fits) to reduce noise in estimates made over time (Deo et al., 2017). Additionally the inclusion of the disturbance history derived from Landsat spectral trajectory has proven effective to boost model performance, particularly given that changes in stand structure are related to time since disturbance (Frazier et al., 2014; Pflugmacher et al., 2012). Moreover, the joint imputation of lidar predictors (e.g., 95th percentile of height) and modelled attributes (e.g., stem volume, aboveground biomass) permits recalculating these attributes as new statistical/allometric models are developed.

5.1. Model performance

We assessed the performance of our model using two approaches. First, we conducted a national assessment using the reserved validation lidar plots according to the reference year in which lidar acquisition was used to inform the model. Second, we applied a temporal assessment using a set of independent lidar acquisitions collected between 2006 and 2012 in the province of Alberta. The results of the national assessment (presented in Table 5) are comparable to those obtained for our single-year (2010) national implementation in Canada's boreal forest (Matasci et al., 2018). R^2 values exceed 0.61 for all attributes, except for those characterizing height variability (both elev_sd and elev_cv), which are irregularly distributed in space, and are thus challenging to model. Caution should be exercised when interpreting the results exclusively based on R^2, as the larger range of attributes values in the hemi-boreal (i.e., more productive ecozones) tends to increase the R^2 response values relative to those reported in Matasci et al. (2018). RMSE% values for gross stem volume and biomass are high and indicate these attributes are challenging to estimate. Both volume and biomass are estimated using allometry, which has inherent associated errors. Estimates for the attributes that are directly measured from lidar had relatively low RMSE% values. Despite the known limitations to using optical data to characterize vertical structure (Duncanson et al., 2010), our model resulted in a RMSE of 2.66 m for mean height. These results indicate an equivalent or superior performance when compared to other studies modelling forest structure combining lidar data and Landsat imagery with a more limited geographic scope. For example, studies conducted in Canadian forested ecosystems modelled mean stand height and reported RMSE values of 3.3 m in central Saskatchewan (Wulder and Seemann, 2003), and 3.24 m in central British Columbia (Varhola and Coops, 2013). Studies in other areas around the world indicated RMSE of 3.01 m in central-west Italy (Maselli et al., 2011), and 1.9–2.3 m in central Spain (Pascual et al., 2010).

In addition to the national validation using the reserved lidar plots, we assessed the temporal transferability of our model using an independent lidar dataset in the province of Alberta, acquired 2006–2012. The results of this assessment (presented in Table 6) indicate that the performance of our model is consistent when applied through time, with RMSE and RMSE% values that are relatively stable across the years. As a comparison, Deo et al. (2017) generated diverse models for aboveground biomass in north-eastern Minnesota, USA. These models were developed considering one or several reference

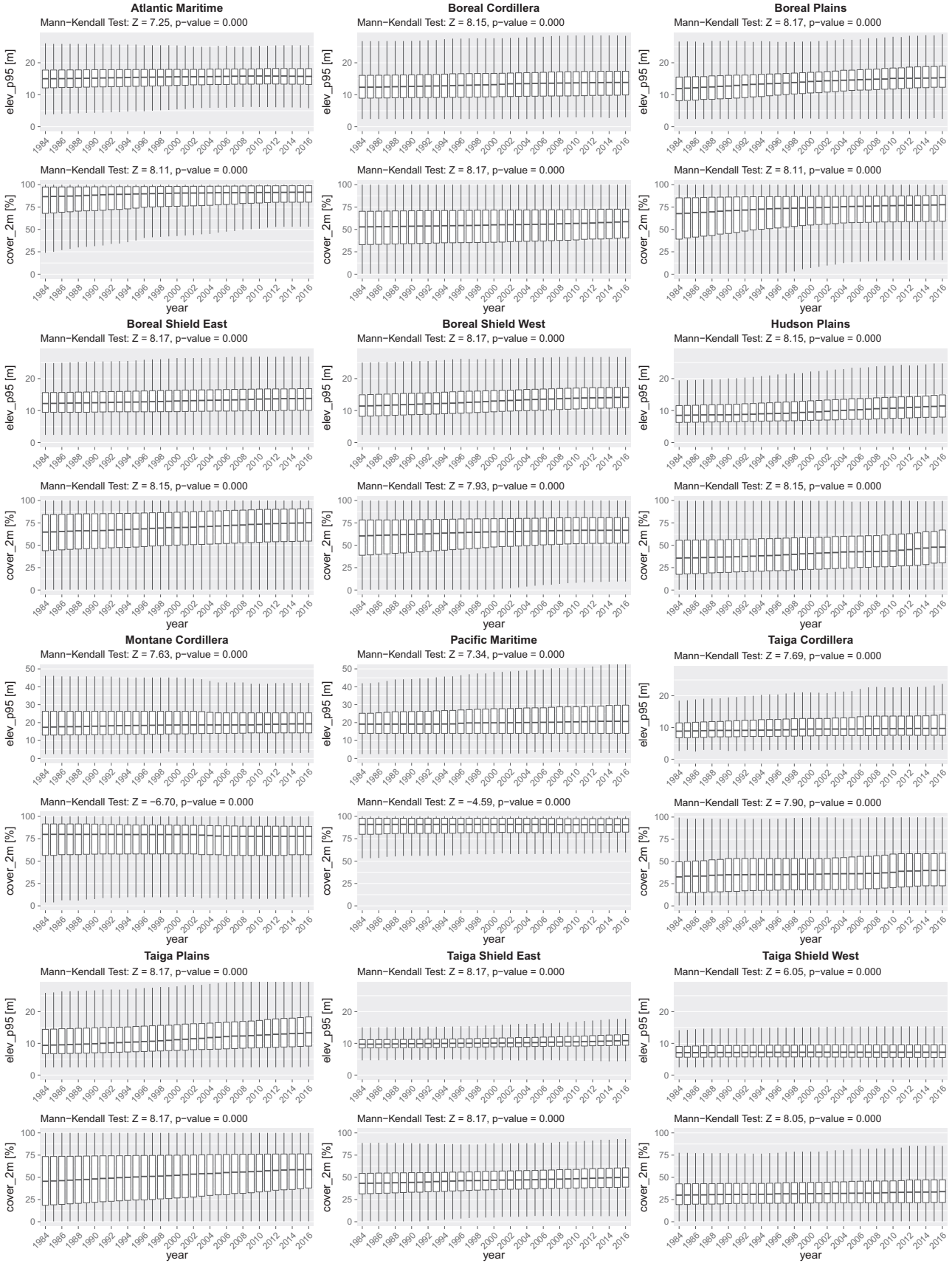

Fig. 4. Canopy height (elev_p95) and canopy cover (cover_2m) dynamics in undisturbed forests in Canada's forested ecozones during 1984–2016. Note the different y-axis scale for elev_p95 for Montane Cordillera and Pacific Maritime.

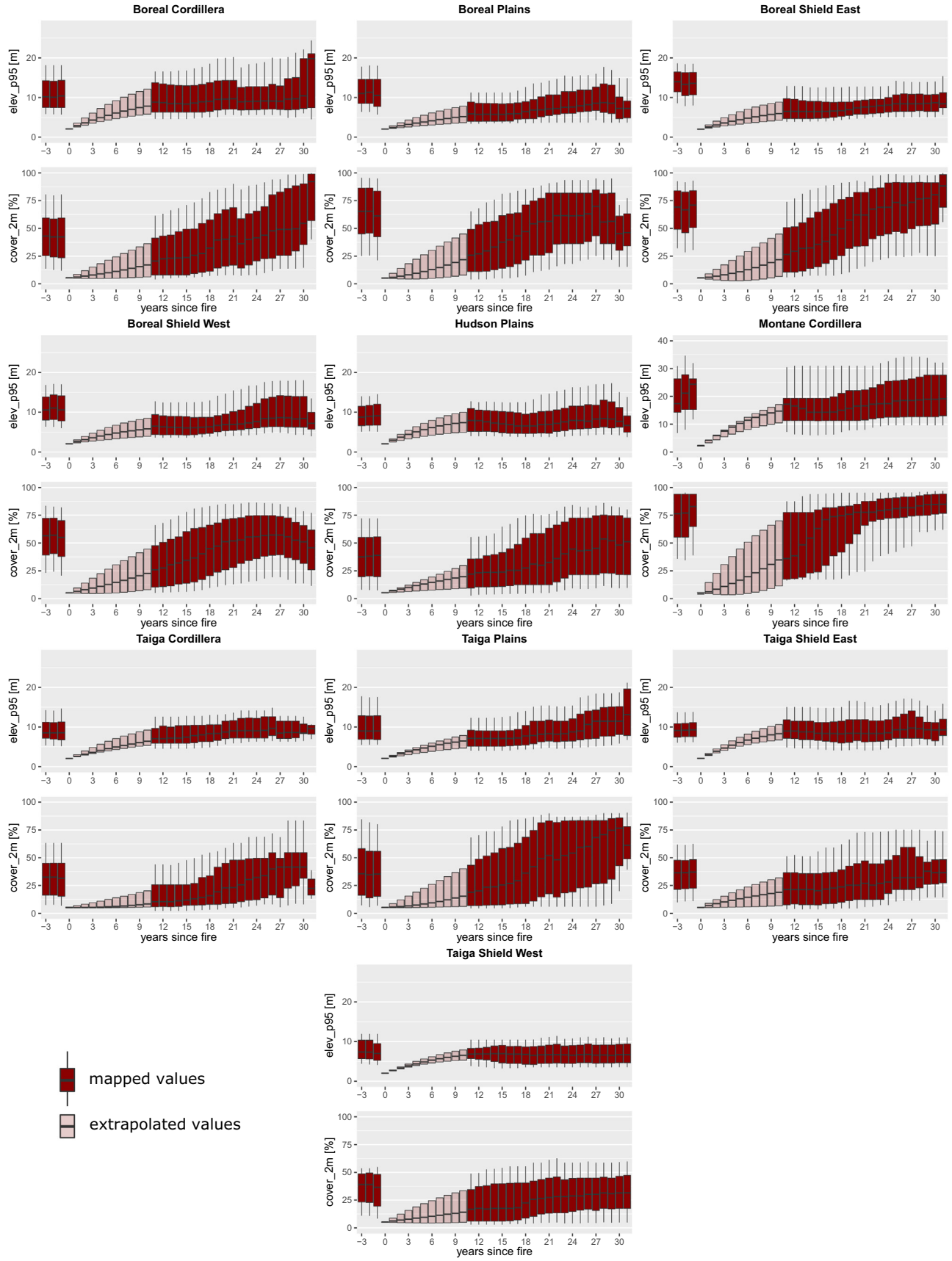

Fig. 5. Distribution of forest structure attributes canopy height (elev_p95) and canopy cover (cover_2m) before and after fire change events by ecozone. Note the different y-axis scale for elev_p95 for Montane Cordillera.

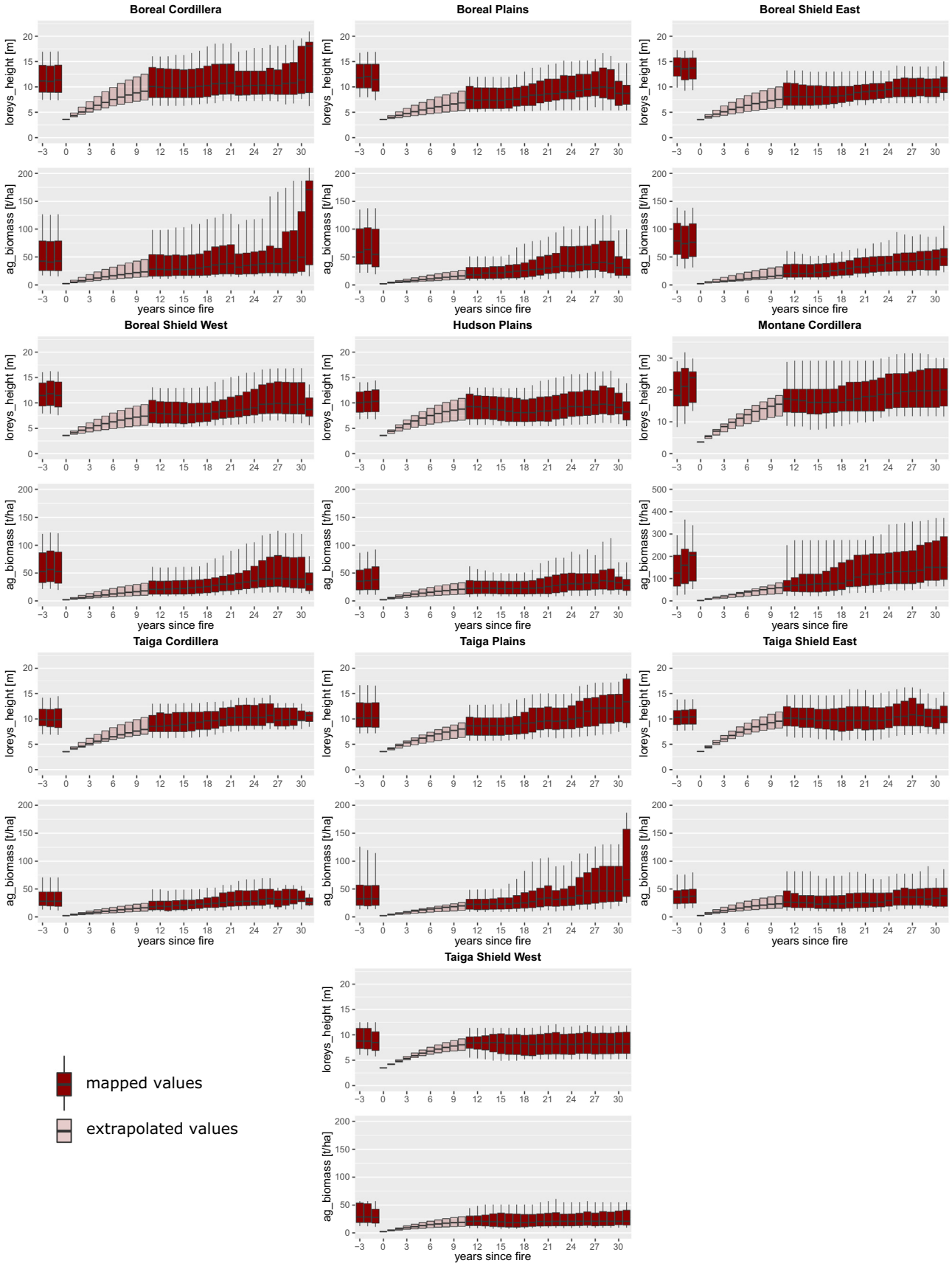

Fig. 6. Distribution of forest structure attributes Lorey's height (loreys_height) and total aboveground biomass (ag_biomass) before and after fire change events by ecozone. Note the different y-axis scale for Montane Cordillera.

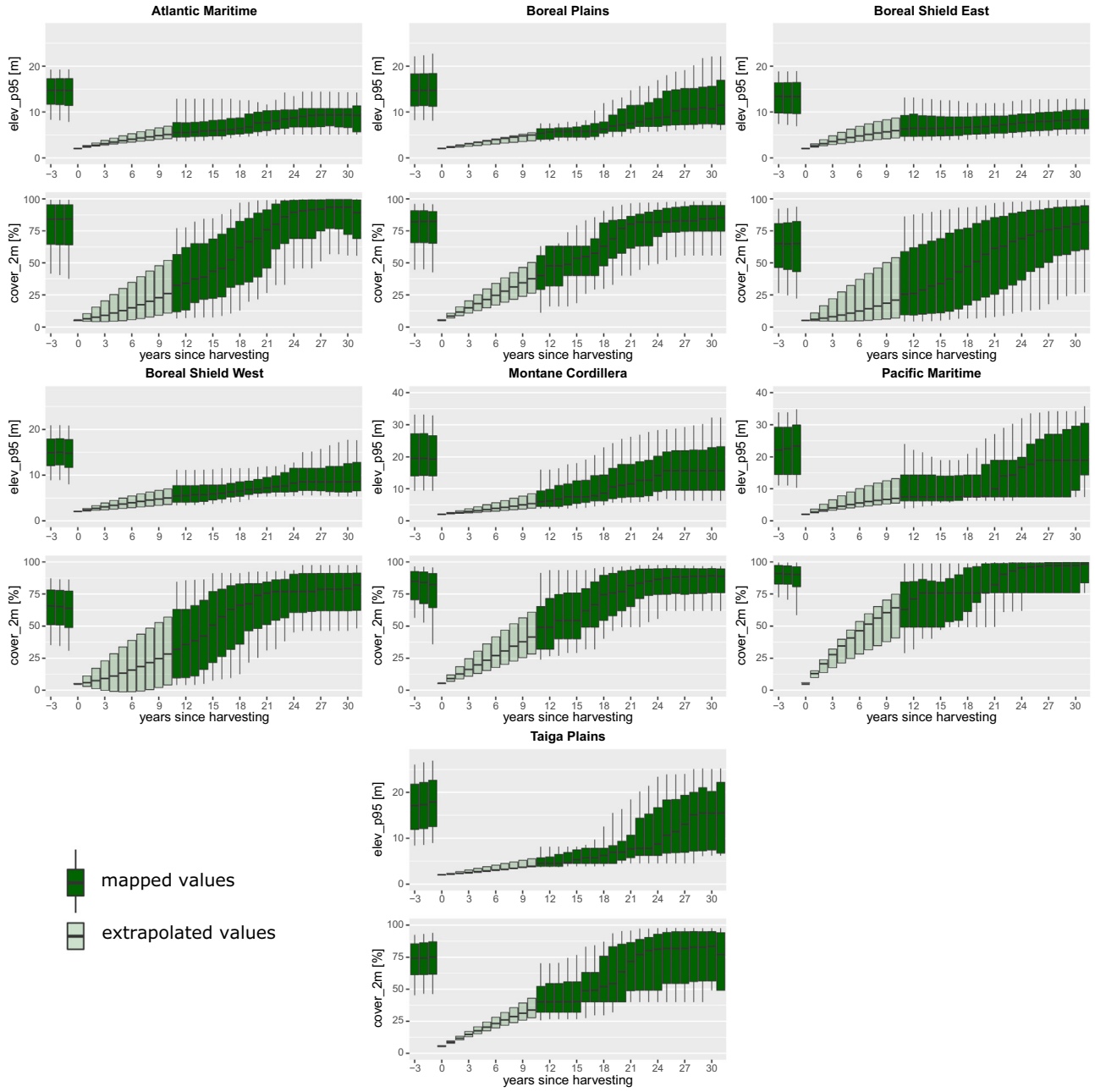

Fig. 7. Distribution of forest structure attributes canopy height (elev_p95) and canopy cover (cover_2m) before and after harvest change events by ecozone. Note the different y-axis scale for elev_p95 for Montane Cordillera and Pacific Maritime.

years and the authors obtained RMSE% ranging from 50.76 to 69.53%. Some of these models where then validated against independent National Forest Inventory (NFI) plot data from 2010 (RMSE% ranging from 68.73 to 72.56%) and 2000 (RMSE% = 75.89%).

These results overall are encouraging and demonstrate that the combination of the two data sources offers significant benefit to understanding how forest stands develop over time. From an operational point of view, the use of Landsat data to generate maps of forest structural metrics is a cost-effective solution to extend lidar estimations through time and space. However, this approach involves trade-offs between the capacity to produce a spatially-explicit, wall-to-wall data layer, and the accuracy of that data layer at any given location. As such, these data provide strategic-level information, but are not considered to have sufficient accuracy to support an operational-level forest inventory. These forest structure products are a valuable source of spatially-explicit information of forest status and dynamics, which can help to complement and enrich existing forest inventory and national monitoring programs, particularly where there is currently a dearth of forest information (White et al., 2014).

5.2. Characterization of forest structure dynamics in Canada's forested ecosystems from 1984 to 2016

Improvements in Landsat data availability and processing routines and capabilities have fostered ongoing research and methodological refinements for land-cover classification using image time-series (Gómez et al., 2016; Hermosilla et al., 2018; Wulder et al., 2018), as well as encouraging studies into forest dynamics at a range of spatial scales from regional (Cohen et al., 2016; Griffiths et al., 2013; Kennedy et al., 2012; Potapov et al., 2015; White et al., 2017) to continental (Hansen et al., 2013; Lehmann et al., 2013) scales. Vegetation successional processes follow known stages towards re-establishment of treed

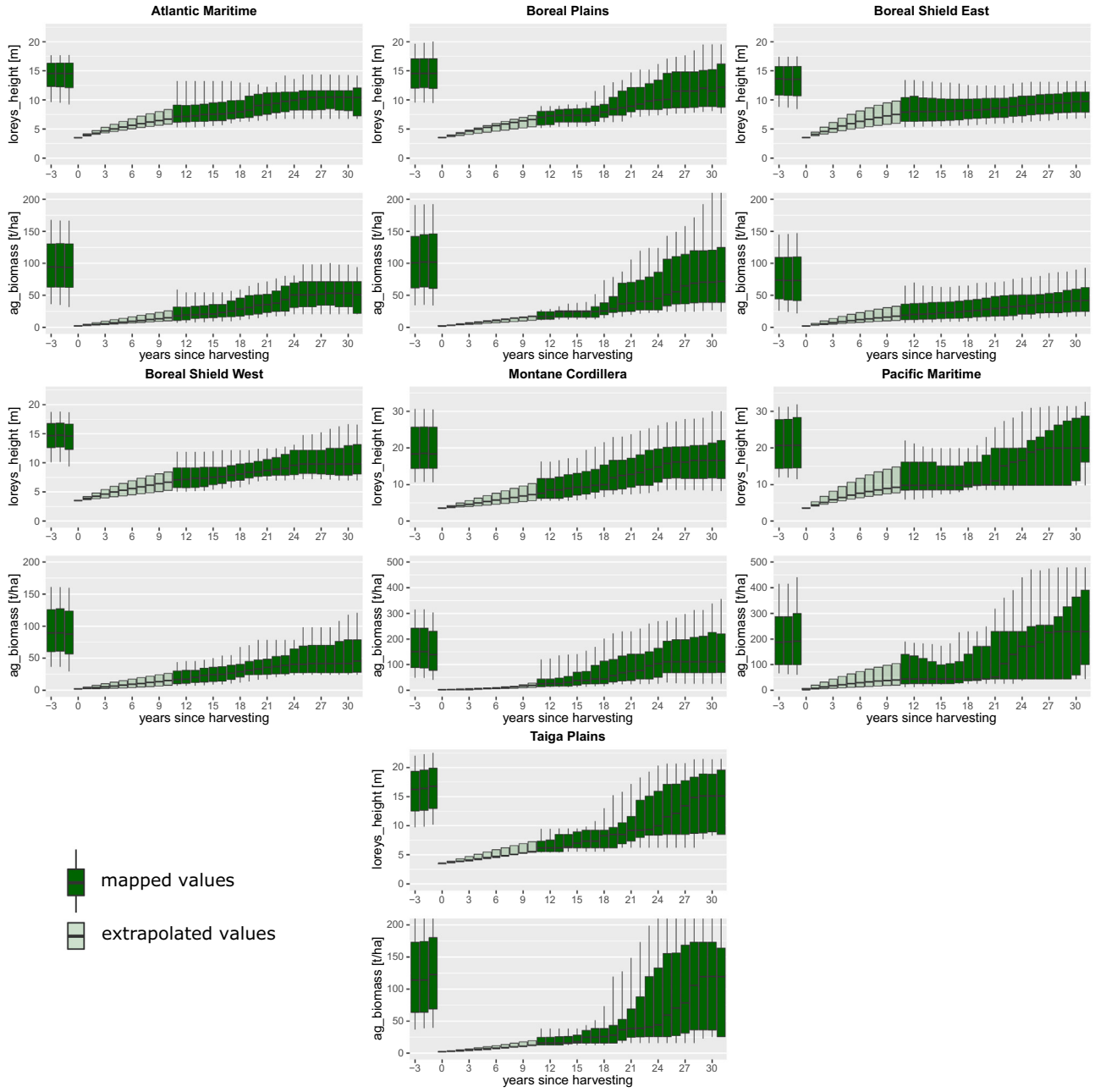

Fig. 8. Distribution of forest structure attributes Lorey's height (loreys_height) and total aboveground biomass (ag_biomass) before and after harvest change events by ecozone. Note the different y-axis scale for Montane Cordillera and Pacific Maritime.

vegetation (Oliver and Larson, 1990), with the spectral wavelengths or indices used providing different indications of recovery (Pickell et al., 2016). Although spectral trends offer insights regarding vegetation recovery (Pickell et al., 2016; White et al., 2017), some spectral measures of recovery do not always correspond to the actual re-establishment of vertically distributed attributes as the vegetation progresses through successional stages from herb and shrub vegetation prior to emergence and dominance of trees and related attributes (e.g., canopy height, biomass) describing forest structure (Griffiths et al., 2013; Kennedy et al., 2012). In this research we have demonstrated that the addition of the comprehensive aboveground vertical characterization provided by lidar to the spatiotemporal rich spectral response provided by Landsat data enables accurate capture and quantification of both the evolution of forest structure and related re-establishment following disturbance events.

The positive, significant trends in both canopy height and canopy cover observed for undisturbed forested areas in Fig. 4 are a result of different stages of stand development, representing both mature and young forests that may have experienced disturbances prior to 1985. Additionally, climatic conditions and site productivity, among other factors, influence the rate at which forests return, with the ecozones showing the strongest trends being located either in the warmer southern or lower-elevation forested ecosystem (i.e., Boreal Plains, Boreal Shield West, Hudson Plains and Taiga Plains). The slight decreasing trends in canopy cover for the Montane Cordillera and Pacific Maritime ecozones (i.e., negative Mann-Kendall test values) can likely be explained by the high canopy cover (cover_2m > 75% throughout the 1984–2016 period) in these two productive ecozones, potentially denoting an opening up of the canopy in more mature forests with denser canopies.

Canopy cover and canopy height display a markedly different response to disturbance events (see Figs. 5 and 7). The results indicating

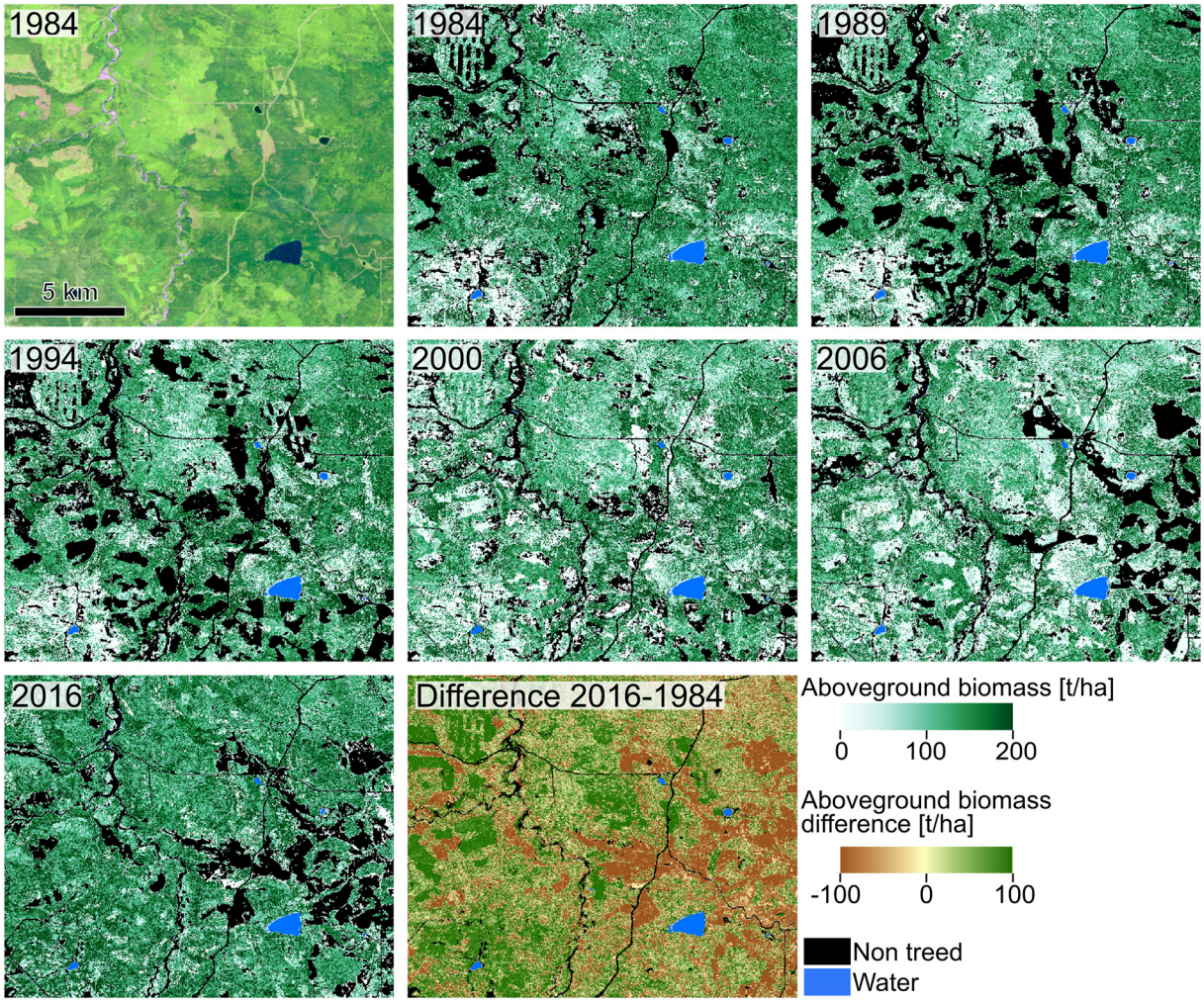

Fig. 9. Temporal evolution of total aboveground biomass (ag_biomass) in 1984, 1989, 1994, 2000, 2006 and 2016, of a sub-region in western Alberta (54° 32′ N/117° 29′ W) with ongoing harvesting activity.

that canopy cover reaches pre-disturbance values earlier (within two decades, on average) than height are likely explained by the rapid development of foliage of residual trees (Bolton et al., 2015). Vertical tree growth and biomass gains are a much slower process (Bartels et al., 2016; Bolton et al., 2017; Harper et al., 2005; Sirois and Payette, 1989), as reflected by the Lorey's height and total aboveground biomass values following disturbance events (see Figs. 6 and 8). The use of temporally varying predictors, in particular time since disturbance, allows the imputation model to identify donor training plots matching the succession stage of the area being mapped.

A different response in the re-establishment of forest vegetation following fire and harvesting events is also observed. In Canada's forests these two stand-replacing disturbances are characterized by distinct recovery patterns (White et al., 2017). Bartels et al. (2016) conducted a meta analysis of published plot data and found that areas impacted by wildfire achieved a benchmark of 10% canopy cover in 5 years, while harvested areas required 10 years to achieve the same benchmark. Both burned and harvested areas were able to achieve height benchmarks of 5 m within 5 years, which may be explained by the fact that regenerating areas are colonized by rapidly growing shade intolerant aspen and pine species after fire. In the longer-term (20 to 30 years), White et al. (2017) found that spectral recovery is more consistent in areas impacted by harvest, as a greater proportion of harvested areas returned to their pre-disturbance spectral values by the end of the analysis period in 2010. While natural regeneration is common in both disturbance types, by law, harvested areas in Canada must be regenerated and are more likely to be subject to systematic replanting and silvicultural activities. Moreover, by definition, harvesting activities occur exclusively over treed sites with greater site productivity, whereas fire occurs over a range of site productivities and land cover types.

Trends for canopy height (elev_p95 and loreys_height) after a fire event (Figs. 5 and 6) can in some cases show a decrease in the early years of the period in which we consider imputed values (10 to 15 years since disturbance) or constant values throughout the whole time-series. The reason for these countertrends is that the 95th height percentile and Lorey's height are sensitive to surviving trees or residual structure (Angers et al., 2011; Bond-Lamberty and Gower, 2008) in the immediate years following disturbance. As time passes, standing dead wood begins to fall, giving way to regrowing trees ultimately resulting in an upward trend (Angers et al., 2011; Chen and Popadiouk, 2002; Harper et al., 2005). Such interpretation is consistent with findings of previous studies of the post-fire recovery in the boreal forest of Canada (Bolton et al., 2017, 2015; Kane et al., 2013).

Currently, there are no spatially explicit national estimates of changes in forest structure in Canada's forests. Canada's NFI is the authoritative source for this information (Gillis et al., 2005); however the NFI baseline was established in 2006 and the first re-measurement data, from which change would be estimated, is not yet complete. Canada's NFI is nominally based on a systematic 1% sample, so estimates of changes in forest structure will be aspatial, stratified by ecozone. The capacity to generate spatially-explicit information products that

characterize changes in forest structure has been demonstrated herein, and offers useful data to augment the information needs of Canada's NFI program (White et al., 2014). As noted earlier, related to limited ongoing jurisdictional monitoring efforts, data needs are particularly acute for Canada's unmanaged northern forest area (Gillis et al., 2005).

5.3. Challenges and limitations for large-area mapping of forest attributes through time

The framework presented in this paper builds on our previous study in which we focused on a single-year model (for 2010) limited to the extent of the Canadian boreal forest (Matasci et al., 2018). To enable that approach to be extended both in time (over a multiple decades) and space (i.e., over the complete extent of the Canadian forested ecosystem, including the hemi-boreal zone), the approach required adaptation, including using a smoothed temporal series of spectral values, and increasing the number and distribution of training samples (lidar plots) to better represent Canada's forested ecosystems.

The main factor enabling the consistent application of a statistical model through both space and time is the use of calibrated physical values (Song et al., 2001). Despite utilizing imagery acquired by three sensors (TM, ETM+ and OLI), the rigorous cross-sensor calibration of the Landsat program (Markham and Helder, 2012) combined with the effectiveness of the radiometric correction procedure applied (Masek et al., 2006), enabled a consistent radiometric response within and between images (Hermosilla et al., 2017, 2015a) over the 1984–2016 period. This normalized surface reflectance dataset constituted a sound foundation for model extension through time and space. However, one of the core challenges we had to overcome was the residual temporal variability existing in the pixel-level spectral time-series, particularly for the estimation of continuous attributes of forest structure (Deo et al., 2017; Pflugmacher et al., 2012). Thus, to enable temporal coherence we used noise-free, trend-fitted, surface reflectance values generated via piecewise linear interpolations resulting from the C2C procedure (Hermosilla et al., 2015a). The use of the trend-fitted reflectance values ensured that the reflectance values used in the training phase and, more importantly, the prediction phase, had limited noise. This mitigated year-to-year fluctuations of the attributes at a local scale in the final maps.

A limitation of the imputation approach is commonly referred to as extrapolation bias. Unlike parametric approaches, imputation cannot extrapolate beyond the minimum and maximum values defined by the calibration data used for model development (Magnussen et al., 2010). As such, it is important that the calibration data represent the full range of forest structure present in the target area of interest. In our case, the full range of forest structural variability in Canada is vast and likely not fully represented by the boreal lidar transect acquired in 2010 and used in Matasci et al. (2018). Consequently, we increased the sample size of lidar plots to ensure representation of the forest conditions found in the hemi-boreal forests of the Montane Cordillera and Pacific Maritime ecozones.

As noted by Zald et al. (2014), although imputation using a single nearest neighbor will conserve the co-variance structure of the response variables, it will also propagate sample-based errors, including measurement error and deficiencies in the sample design. In the context of volume and biomass, allometric error is also an issue (Duncanson et al., 2015). Potential approaches to accurately quantify and propagate these errors are emerging (Sexton et al., 2015; Wayson et al., 2015). An avenue to investigate could be that of leveraging the capability of ensemble approaches to characterize uncertainty (Kennedy et al., 2018), although this may not be readily implemented for such large-area assessments.

Another challenge involves accounting for the impact of low magnitude, variable temporal persistence, non-stand replacing disturbances (such as from drought or defoliating insects). These disturbances typically represent changes in forest condition (Hall et al., 2016), rather than removal of the forest as is traditionally the case with stand-replacing fire and harvest (Hermosilla et al., 2015b). Multiple factors can contribute to a general state of forest decline in any given area (Cohen et al., 2016), further complicating disturbance attribution (Hermosilla et al., 2015b; Zhu, 2017) and determination of subsequent impacts (Kurz et al., 2013). In Canada, the area impacted by non-stand replacing disturbances, particularly insects, on an annual basis often exceeds that of wildfire and harvest (Wulder et al., 2007). As reported by Stinson et al. (2011), insects often cause only partial mortality in the stand, and therefore the impacts of insects on biomass carbon stocks are far smaller than the impacts of fire or harvest. In extreme circumstances, however, such as with the mountain pine beetle infestation in British Columbia in the 2000's, an epidemic infestation can have large biomass consequences (Kurz et al., 2008). Insect damage often provides increased fuels for subsequent wildfires (Kurz et al., 2013; Stinson et al., 2011). Determining appropriate methods and approaches to incorporate the impacts of these non-stand replacing disturbances on our estimates is a topic for future research.

5.4. Opportunities and future directions

There are opportunities that can improve the performance and robustness of the spatio-temporal workflow for wall-to-wall mapping of forest attributes at a 30 m spatial resolution presented herein. Future work could involve the refinement of the prediction models used to derive the forest structural attributes (such as gross stem volume and total aboveground biomass) from the lidar data. Non-parametric models are increasingly used to derive forest structure metrics from lidar observations, as they do not have restrictive assumptions on the data analyzed (Penner et al., 2013). Access to additional lidar datasets may help to augment the representation of forest structure in more varied ecological and disturbance-related conditions, which in turn may improve the estimation of structural attributes across Canada's forested ecosystems using the methods presented herein. With these improvements in mind, besides internal efforts, activities to partner with provincial and territorial resource management agencies to augment ground plot holdings and access additional lidar datasets are on-going.

The use of additional spectral data acquired beyond the current compositing window (August 1 ± 30 days) and representing within-year variation in vegetation phenology may aid in reducing issues associated with asymptotic responses for attributes such as biomass (Zhu and Liu, 2015). Future work may involve the production of a time series of within-year BAP Landsat composites and associated spectral metrics that capture within-year variations. This opportunity, however, might be hindered by historical data availability (White and Wulder, 2014), as well as a greater likelihood of cloud cover, which can confound compositing approaches (White et al., 2014).

Time since disturbance has previously been demonstrated to be a valuable predictor of forest structure (Matasci et al., 2018; Zald et al., 2016) as it informs on the recovery and successional stage reached by the developing stands (Pflugmacher et al., 2012). Currently, this indicator is limited by the availability of 30-m Landsat data. Augmenting the time-series to incorporate Landsat Multispectral Scanner System (MSS) imagery could extend the monitoring period to as early as 1972 (Vogeler et al., 2018). Alternatively, other mapped forest change data, such as the Canadian National Fire Database, could be incorporated to provide information on disturbances prior 1985.

6. Conclusions

Demands for forest information are increasing for a broad range of applications. Information must be spatially explicit and characterize forest dynamics at a scale that captures anthropogenic impacts. Herein, the incorporation of Landsat and lidar data provides key forest structural variables that satisfy this information need, with spatial layers that have been generated in a consistent and transparent manner

through time and over large spatial extents. To do so, a NN statistical imputation model based on RF was built based upon these two complementary sources of remotely sensed data. A set of wall-to-wall predictor variables from Landsat pixel composites was combined with positional and topographic information as well as with a pixel-based disturbance history to model the forest attributes derived from lidar acquisitions. Leveraging the available multi-decadal time-series of Landsat data, the model allowed us to exhaustively and annually map forest structural attributes at a 30 m resolution from 1984 to 2016 over the entire ~650 million ha forested ecosystem of Canada. The validation of the model on independent plots resulted in outcomes that are comparable to previously published studies, including prior work on a single-year estimate for the entire boreal forest of Canada (Matasci et al., 2018). The unique contributions of the research presented herein can be summarized as follows. First, this effort represents a further building block towards attaining operational capacity for large-area forest monitoring programs. Starting from a prototype study focusing on a small area (Zald et al., 2016), we extended the spatial and temporal scale of the modelling framework to ultimately demonstrate its efficacy and robustness at the desired scale of implementation: the entire forested area of Canada over a time period spanning three decades. Second, we implemented an independent stand-level validation of the estimates over multiple years using lidar data that was not used in the model development. This unique temporally representative validation exercise builds confidence in the portability of our models through time. Third, we showed how the resultant time-series of spatial layers enable the study of forest growth and recovery after disturbance across Canada. We offer insights on stand dynamics by capturing the regional patterns of Canada's various forested ecosystems, by examining the behavior of distinct structural forest attributes, and by comparing the response after fire and harvesting events. Given similar information needs and forest conditions, the approach demonstrated here is portable and subject to widespread implementation due to the increasing availability of the datasets used and cloud based computing infrastructure.

Acknowledgments

This research was undertaken as part of the “Earth Observation to Inform Canada's Climate Change Agenda (EO3C)” project jointly funded by the Canadian Space Agency (CSA), Government Related Initiatives Program (GRIP), and the Canadian Forest Service (CFS) of Natural Resources Canada. This research was enabled in part by support provided by WestGrid (www.westgrid.ca) and Compute Canada (www.computecanada.ca). This work has also been supported by a mobility grant offered by the University of Lausanne, Switzerland, for the project titled: “Fusion of lidar and optical remote sensing data for forestry applications: a machine learning approach”. The authors wish to thank Dave Lasser (Sunshine Coast Community Forest), Ken Day and Cathy Koot (Alex Fraser Research Forest), Benoit St-Onge (Université du Québec à Montréal), Jerry Maedel (University of British Columbia), and Ionut Aron (Malcolm Knapp Research Forest) for supplying critical lidar datasets. Additionally, Christopher Hopkinson (University of Lethbridge) is thanked for efforts in collecting and processing the boreal wide lidar transects used in this study.

References

Abercrombie, S.P., Friedl, M.A., 2016. Improving the consistency of multitemporal land cover maps using a hidden Markov model. IEEE Trans. Geosci. Remote Sens. 54, 703–713. https://doi.org/10.1109/TGRS.2015.2463689.

Ahmed, O.S., Franklin, S.E., Wulder, M.A., White, J.C., 2015. Characterizing stand-level forest canopy cover and height using Landsat time series, samples of airborne LiDAR, and the Random Forest algorithm. ISPRS J. Photogramm. Remote Sens. 101, 89–101. https://doi.org/10.1016/j.isprsjprs.2014.11.007.

Angers, V.A., Gauthier, S., Drapeau, P., Jayen, K., Bergeron, Y., 2011. Tree mortality and snag dynamics in North American boreal tree species after a wildfire: a long-term study. Int. J. Wildland Fire 20, 751–763. https://doi.org/10.1071/WF10010.

Bartels, S.F., Chen, H.Y.H., Wulder, M.A., White, J.C., 2016. Trends in post-disturbance recovery rates of Canada's forests following wildfire and harvest. For. Ecol. Manag. 361, 194–207. https://doi.org/10.1016/j.foreco.2015.11.015.

Bater, C., Coops, N.C., Gergel, S.E., Lemay, V.M., Collins, D., 2009. Estimation of standing dead tree class distributions in northwest coastal forests using lidar remote sensing. Can. J. For. Res. 39, 1080–1091. https://doi.org/10.1139/X09-030.

Bater, C.W., Wulder, M.A., Coops, N.C., Hopkinson, C., Coggins, S.B., Arsenault, E., Beaudoin, A., Guindon, L., Hall, R.J., Villemaire, P., Woods, M., 2011. Model development for the estimation of aboveground biomass using a lidar-based sample of Canada's boreal forest. In: SilviLaser. Hobart, Tasmania, Australia, pp. 8.

Beaudoin, A., Bernier, P.Y., Guindon, L., Villemaire, P., Guo, X.J., Stinson, G., Bergeron, T., Magnussen, S., Hall, R.J., 2014. Mapping attributes of Canada's forests at moderate resolution through *k* NN and MODIS imagery. Can. J. For. Res. 44, 521–532. https://doi.org/10.1139/cjfr-2013-0401.

Belward, A.S., Skøien, J.O., 2014. Who launched what, when and why; trends in global land-cover observation capacity from civilian earth observation satellites. ISPRS J. Photogramm. Remote Sens. 103, 115–128. https://doi.org/10.1016/j.isprsjprs.2014.03.009.

Beven, K.J., Kirkby, M.J., 1979. A physically based, variable contributing area model of basin hydrology. Hydrol. Sci. Bull. 24, 43–69. https://doi.org/10.1080/02626667909491834.

Boisvenue, C., Smiley, B.P., White, J.C., Kurz, W.A., Wulder, M.A., 2016. Improving carbon monitoring and reporting in forests using spatially-explicit information. Carbon Balance Manag. 11, 23. https://doi.org/10.1186/s13021-016-0065-6.

Bolton, D.K., Coops, N.C., Wulder, M.A., 2015. Characterizing residual structure and forest recovery following high-severity fire in the western boreal of Canada using Landsat time-series and airborne lidar data. Remote Sens. Environ. 163, 48–60.

Bolton, D.K., Coops, N.C., Hermosilla, T., Wulder, M.A., White, J.C., 2017. Assessing variability in post-fire forest structure along gradients of productivity in the Canadian boreal using multi-source remote sensing. J. Biogeogr. 44 (6), 1294–1305. https://doi.org/10.1111/jbi.12947.

Bolton, D.K., White, J.C., Wulder, M.A., Coops, N.C., 2018. Updating stand-level forest inventories using airborne laser scanning and Landsat time series data. Int. J. Appl. Earth Obs. Geoinf. 66, 174–183. https://doi.org/10.1016/j.jag.2017.11.016.

Bond-Lamberty, B., Gower, S.T., 2008. Decomposition and fragmentation of coarse woody debris: re-visiting a boreal black spruce chronosequence. Ecosystems 11, 831–840. https://doi.org/10.1007/s10021-008-9163-y.

Brandt, J.P., 2009. The extent of the North American boreal zone. Environ. Rev. 17, 101–161. https://doi.org/10.1139/A09-004.

Breiman, L., 2001. Random forests. Mach. Learn. 45, 5–32.

Chen, H.Y., Popadiouk, R.V., 2002. Dynamics of North American boreal mixedwoods. Environ. Rev. 10, 137–166. https://doi.org/10.1139/a02-007.

Cihlar, J., 2000. Land cover mapping of large areas from satellites: status and research priorities. Int. J. Remote Sens. 21, 1093–1114. https://doi.org/10.1080/014311600210092.

Cohen, W.B., Yang, Z., Stehman, S.V., Schroeder, T.A., Bell, D.M., Masek, J.G., Huang, C., Meigs, G.W., 2016. Forest disturbance across the conterminous United States from 1985–2012: the emerging dominance of forest decline. For. Ecol. Manag. 360, 242–252. https://doi.org/10.1016/j.foreco.2015.10.042.

Coops, N.C., Hilker, T., Wulder, M.A., St-Onge, B., Newnham, G.J., Siggins, A., Trofymow, J.A., 2007. Estimating canopy structure of Douglas-fir forest stands from discrete-return LiDAR. Trees-Struct. Funct. 21, 295–310. https://doi.org/10.1007/s00468-006-0119-6.

Coops, N.C., Duffe, J., Koot, C., 2010. Assessing the utility of lidar remote sensing technology to identify mule deer winter habitat. Can. J. Remote Sens. 36, 81–88. https://doi.org/10.5589/m10-029.

Coops, N.C., Tompalski, P., Nijland, W., Rickbeil, G.J.M., Nielsen, S.E., Bater, C.W., Stadt, J.J., 2016. A forest structure habitat index based on airborne laser scanning data. Ecol. Indic. 67, 346–357. https://doi.org/10.1016/j.ecolind.2016.02.057.

Crist, E., 1985. A TM tasseled cap equivalent transformation for reflectance factor data. Remote Sens. Environ. 306, 301–306.

Crookston, N.L., Finley, A.O., 2008. yaImpute: an R package for kNN imputation. J. Stat. Softw. 23, 1–16.

Daily, G.C., 1997. Nature's Services, Island Press. Island Press, Washington D.C.

Deo, R.K., Russell, M.B., Domke, G.M., Woodall, C.W., Falkowski, M.J., Cohen, W.B., 2017. Using Landsat time-series and LiDAR to inform aboveground forest biomass baselines in Northern Minnesota, USA. Can. J. Remote Sens. 43, 28–47. https://doi.org/10.1080/07038992.2017.1259556.

Duncanson, L.I., Niemann, K.O., Wulder, M.A., 2010. Integration of GLAS and Landsat TM data for aboveground biomass estimation. Can. J. Remote Sens. 36, 129–141.

Duncanson, L.I., Dubayah, R.O., Enquist, B.J., 2015. Assessing the general patterns of forest structure: quantifying tree and forest allometric scaling relationships in the United States. Glob. Ecol. Biogeogr. 24, 1465–1475. https://doi.org/10.1111/geb.12371.

Ecological Stratification Working Group, 1996. A national ecological framework for Canada. Agriculture and Agri-Food Canada and Environment Canada, Ottawa, ON (Available from: http://sis.agr.gc.ca/cansis/publications/ecostrat/cad_report.pdf [cited on May 12th 2018]).

Eskelson, B.N.I., Temesgen, H., Lemay, V., Barrett, T.M., Crookston, N.L., Hudak, A.T., 2009. The roles of nearest neighbor methods in imputing missing data in forest inventory and monitoring databases. Scand. J. For. Res. 24, 235–246. https://doi.org/10.1080/02827580902870490.

Fekety, P.A., Falkowski, M.J., Hudak, A.T., 2014. Temporal transferability of LiDAR-based imputation of forest inventory attributes. Can. J. For. Res. 45, 422–435. https://doi.org/10.1139/cjfr-2014-0405.

Frazier, R.J., Coops, N.C., Wulder, M.A., Kennedy, R., 2014. Characterization of

aboveground biomass in an unmanaged boreal forest using Landsat temporal segmentation metrics. ISPRS J. Photogramm. Remote Sens. 92, 137–146.
Frazier, R.J., Coops, N.C., Wulder, M.A., 2015. Boreal shield forest disturbance and recovery trends using Landsat time series. Remote Sens. Environ. 170, 317–327. https://doi.org/10.1016/j.rse.2015.09.015.
Frolking, S., Palace, M.W., Clark, D.B., Chambers, J.Q., Shugart, H.H., Hurtt, G.C., 2009. Forest disturbance and recovery: a general review in the context of spaceborne remote sensing of impacts on aboveground biomass and canopy structure. J. Geophys. Res. Biogeosci. 114. https://doi.org/10.1029/2008JG000911.
Gillis, M., Omule, A., Brierley, T., 2005. Monitoring Canada's forests: the National Forest Inventory. For. Chron. 81, 214–221. https://doi.org/10.5558/tfc81214-2.
Gleason, C.J., Im, J., 2012. Forest biomass estimation from airborne LiDAR data using machine learning approaches. Remote Sens. Environ. 125, 80–91.
Gómez, C., White, J.C., Wulder, M.A., 2016. Optical remotely sensed time series data for land cover classification: a review. ISPRS J. Photogramm. Remote Sens. 116, 55–72. https://doi.org/10.1016/j.isprsjprs.2016.03.008.
Griffiths, P., Van Der Linden, S., Kuemmerle, T., Hostert, P., 2013. A pixel-based Landsat compositing algorithm for large area land cover mapping. IEEE J. Sel. Top. Appl. Earth Obs. Remote Sens. 6, 2088–2101.
Hall, R.J., Castilla, G., White, J.C., Cooke, B.J., Skakun, R.S., 2016. Remote sensing of forest pest damage: a review and lessons learned from a Canadian perspective. Can. Entomol. 148, S296–S356. https://doi.org/10.4039/tce.2016.11.
Hansen, M.C., Loveland, T.R., 2012. A review of large area monitoring of land cover change using Landsat data. Remote Sens. Environ. 122, 66–74. https://doi.org/10.1016/j.rse.2011.08.024.
Hansen, M.C., Potapov, P.V., Moore, R., Hancher, M., Turubanova, S.A., Tyukavina, A., Thau, D., Stehman, S.V., Goetz, S.J., Loveland, T.R., Kommareddy, A., Egorov, A., Chini, L., Justice, C.O., Townshend, J.R.G., 2013. High-resolution global maps of 21st-century forest cover change. Science 342, 850–853. https://doi.org/10.1126/science.1244693.
Harper, K.A., Bergeron, Y., Drapeau, P., Gauthier, S., De Grandpré, L., 2005. Structural development following fire in black spruce boreal forest. For. Ecol. Manag. 206, 293–306. https://doi.org/10.1016/j.foreco.2004.11.008.
Hermosilla, T., Wulder, M.A., White, J.C., Coops, N.C., Hobart, G.W., 2015a. An integrated Landsat time series protocol for change detection and generation of annual gap-free surface reflectance composites. Remote Sens. Environ. 158, 220–234. https://doi.org/10.1016/j.rse.2014.11.005.
Hermosilla, T., Wulder, M.A., White, J.C., Coops, N.C., Hobart, G.W., 2015b. Regional detection, characterization, and attribution of annual forest change from 1984 to 2012 using Landsat-derived time-series metrics. Remote Sens. Environ. 170, 121–132. https://doi.org/10.1016/j.rse.2015.09.004.
Hermosilla, T., Wulder, M.A., White, J.C., Coops, N.C., Hobart, G.W., Campbell, L.B., 2016. Mass data processing of time series Landsat imagery: pixels to data products for forest monitoring. Int. J. Digital Earth 9, 1035–1054. https://doi.org/10.1080/17538947.2016.1187673.
Hermosilla, T., Wulder, M.A., White, J.C., Coops, N.C., Hobart, G.W., 2017. Updating Landsat time series of surface-reflectance composites and forest change products with new observations. Int. J. Appl. Earth Obs. Geoinf. 63, 104–111. https://doi.org/10.1016/j.jag.2017.07.013.
Hermosilla, T., Wulder, M.A., White, J.C., Coops, N.C., Hobart, G.W., 2018. Disturbance-informed annual land cover classification maps of Canada's forested ecosystems for a 29-year Landsat time series. Can. J. Remote Sens. 44 (1), 67–87. https://doi.org/10.1080/07038992.2018.1437719.
Holben, B.N., 1986. Characteristics of maximum-value composite images from temporal AVHRR data. Int. J. Remote Sens. 7, 1417–1434. https://doi.org/10.1080/01431168608948945.
Hudak, A.T., Crookston, N.L., Evans, J.S., Hall, D.E., Falkowski, M.J., 2008. Nearest neighbor imputation of species-level, plot-scale forest structure attributes from LiDAR data. Remote Sens. Environ. 112, 2232–2245.
Kane, V.R., Lutz, J.A., Roberts, S.L., Smith, D.F., McGaughey, R.J., Povak, N.A., Brooks, M.L., 2013. Landscape-scale effects of fire severity on mixed-conifer and red fir forest structure in Yosemite National Park. For. Ecol. Manag. 287, 17–31. https://doi.org/10.1016/j.foreco.2012.08.044.
Kangas, A., Maltamo, M., 2006. Forest Inventory. Methodology and Applications. Springer.
Kendall, M.G., 1955. Rank Correlation Methods. Hafner Publishing Co., New York.
Kennedy, R.E., Yang, Z., Cohen, W.B., Pfaff, E., Braaten, J., Nelson, P., 2012. Spatial and temporal patterns of forest disturbance and regrowth within the area of the Northwest Forest Plan. Remote Sens. Environ. 122, 117–133. https://doi.org/10.1016/j.rse.2011.09.024.
Kennedy, R.E., Ohmann, J., Gregory, M., Roberts, H., Yang, Z., Bell, D.M., Kane, V., Hughes, M.J., Cohen, W.B., Powell, S., Neeti, N., Larrue, T., Hooper, S., Kane, J., Miller, D.L., Perkins, J., Braaten, J., Seidl, R., 2018. An empirical, integrated forest biomass monitoring system. Environ. Res. Lett. 13. https://doi.org/10.1088/1748-9326/aa9d9e.
Key, C.H., Benson, N.C., 2006. Landscape assessment: sampling and analysis methods. USDA For. Serv. Gen. Tech. Rep. 1–55 (RMRS-GTR-164-CD).
Kovalskyy, V., Roy, D.P., 2013. The global availability of Landsat 5 TM and Landsat 7 ETM+ land surface observations and implications for global 30 m Landsat data product generation. Remote Sens. Environ. 130, 280–293. https://doi.org/10.1016/j.rse.2012.12.003.
Kurz, W.A., Dymond, C.C., Stinson, G., Rampley, G.J., Neilson, E.T., Carroll, A.L., Ebata, T., Safranyik, L., 2008. Mountain pine beetle and forest carbon feedback to climate change. Nature 452, 987–990. https://doi.org/10.1038/nature06777.
Kurz, W.A., Dymond, C.C., White, T., Stinson, G., Shaw, C.H., Rampley, G.J., Smyth, C., Simpson, B.N., Neilson, E.T., Trofymow, J.A., Metsaranta, J., Apps, M.J., 2009. CBM-CFS3: a model of carbon-dynamics in forestry and land-use change implementing IPCC standards. Ecol. Model. 220, 480–504. https://doi.org/10.1016/j.ecolmodel.2008.10.018.
Kurz, W.A., Shaw, C.H., Boisvenue, C., Stinson, G., Metsaranta, J., Leckie, D., Dyk, A., Smyth, C., Neilson, E.T., 2013. Carbon in Canada's boreal forest—a synthesis. Environ. Rev. 21, 260–292. https://doi.org/10.1080/1366879042000332970.
Lambert, M.-C., Ung, C.-H., Raulier, F., 2005. Canadian national tree aboveground biomass equations. Can. J. For. Res. 35, 1996–2018. https://doi.org/10.1139/x05-112.
Latifi, H., Nothdurft, A., Koch, B., 2010. Non-parametric prediction and mapping of standing timber volume and biomass in a temperate forest: application of multiple optical/LiDAR-derived predictors. Forestry 83, 395–407.
Lehmann, E.A., Wallace, J.F., Caccetta, P.A., Furby, S.L., Zdunic, K., 2013. Forest cover trends from time series Landsat data for the Australian continent. Int. J. Appl. Earth Obs. Geoinf. 21, 453–462. https://doi.org/10.1016/j.jag.2012.06.005.
Liaw, A., Wiener, M., 2002. Classification and regression by randomForest. R news 2, 18–22.
Lu, Y., Coops, N.C., Bolton, D.K., Wang, T., Wang, G., 2015. Comparing stem volume predictions of coastal Douglas-fir stands in British Columbia using a simple physiological model and LiDAR remote sensing. For. Sci. 61, 586–596. https://doi.org/10.5849/forsci.13-197.
MacDicken, K.G., 2015. Global forest resources assessment 2015: what, why and how? For. Ecol. Manag. 352, 3–8. https://doi.org/10.1016/j.foreco.2015.02.006.
Magnussen, S., Tomppo, E., McRoberts, R.E., 2010. A model-assisted k-nearest neighbour approach to remove extrapolation bias. Scand. J. For. Res. 25, 174–184. https://doi.org/10.1080/02827581003667348.
Mann, H.B., 1945. Nonparametric tests against trend. Econometrica 13, 245–259.
Markham, B.L., Helder, D.L., 2012. Forty-year calibrated record of earth-reflected radiance from Landsat: a review. Remote Sens. Environ. 122, 30–40. https://doi.org/10.1016/j.rse.2011.06.026.
Marshall, P., Lemay, V., 2006. Forest inventory. In: Forestry Handbook for British Columbia. The Forestry Undergraduate Society, Faculty of Forestry, University of British Columbia, Vancouver, BC, pp. 577–604. https://doi.org/10.1007/1-4020-4381-3.
Masek, J.G., Vermote, E.F., Saleous, N.E., Wolfe, R., Hall, F.G., Huemmrich, K.F., Gao, F., Kutler, J., Lim, T.K., 2006. A Landsat surface reflectance dataset for North America, 1990–2000. IEEE Geosci. Remote Sens. Lett. 3, 68–72.
Masek, J.G., Cohen, W.B., Leckie, D., Wulder, M.A., Vargas, R., de Jong, B., Healey, S., Law, B., Birdsey, R., Houghton, R.A., Mildrexler, D., Goward, S., Smith, W.B., 2011. Recent rates of forest harvest and conversion in North America. J. Geophys. Res. 116, 1–22. https://doi.org/10.1029/2010JG001471.
Maselli, F., Chiesi, M., Montaghi, A., Pranzini, E., 2011. Use of ETM+ images to extend stem volume estimates obtained from lidar data. ISPRS J. Photogramm. Remote Sens. 66, 662–671. https://doi.org/10.1016/j.isprsjprs.2011.04.007.
Matasci, G., Hermosilla, T., Wulder, M.A., White, J.C., Coops, N.C., Hobart, G.W., Zald, H.S., 2018. Large-area mapping of Canadian boreal forest cover, height, biomass and other structural attributes using Landsat composites and lidar plots. Remote Sens. Environ. 209, 90–106.
McGaughey, R.J., 2013. FUSION/LDV: Software for LIDAR Data Analysis and Visualization. US Department of Agriculture, Forest Service, Pacific Northwest Research Station, Seattle, WA.
Næsset, E., 1997. Estimating timber volume of forest stands using airborne laser scanner data. Remote Sens. Environ. 61, 246–253. https://doi.org/10.1016/S0034-4257(97)00041-2.
Næsset, E., 2002. Predicting forest stand characteristics with airborne scanning laser using a practical two-stage procedure and field data. Remote Sens. Environ. 80, 88–99. https://doi.org/10.1016/S0034-4257(01)00290-5.
Natural Resources Canada, 2016. The State of Canada's Forests: Annual Report 2016. Ottawa. .
Natural Resources Canada, 2017. The state of Canada's forests: Annual Report 2017. Ottawa. .
Ohmann, J.L., Gregory, M.J., 2002. Predictive mapping of forest composition and structure with direct gradient analysis and nearest-neighbor imputation in coastal Oregon, USA. Can. J. For. Res. 32, 725–741.
Oliver, C.D., Larson, B.C., 1990. Forest Stand Dynamics. John Wiley and Sons, New York, NY.
Pascual, C., García-Abril, A., Cohen, W.B., Martín-Fernández, S., 2010. Relationship between LiDAR-derived forest canopy height and Landsat images. Int. J. Remote Sens. 31, 1261–1280. https://doi.org/10.1080/01431160903380656.
Penner, M., Pitt, D.G., Woods, M.E., 2013. Parametric vs. nonparametric LiDAR models for operational forest inventory in boreal Ontario. Can. J. Remote Sens. 39, 426–443. https://doi.org/10.5589/m13-049.
Pflugmacher, D., Cohen, W.B., Kennedy, R.E., 2012. Using Landsat-derived disturbance history (1972–2010) to predict current forest structure. Remote Sens. Environ. 122, 146–165. https://doi.org/10.1016/j.rse.2011.09.025.
Pflugmacher, D., Cohen, W.B., Kennedy, R.E., Yang, Z., 2014. Using Landsat-derived disturbance and recovery history and lidar to map forest biomass dynamics. Remote Sens. Environ. 151, 124–137.
Pickell, P.D., Hermosilla, T., Frazier, R.J., Coops, N.C., Wulder, M.A., 2016. Forest recovery trends derived from Landsat time series for North American boreal forests. Int. J. Remote Sens. 37, 138–149. https://doi.org/10.1080/2150704X.2015.1126375.
Potapov, P.V., Turubanova, S.A., Tyukavina, A., Krylov, A.M., McCarty, J.L., Radeloff, V.C., Hansen, M.C., 2015. Eastern Europe's forest cover dynamics from 1985 to 2012 quantified from the full Landsat archive. Remote Sens. Environ. 159, 28–43. https://doi.org/10.1016/j.rse.2014.11.027.
Price, D.T., Alfaro, R.I., Brown, K.J., Flannigan, M.D., Fleming, R.A., Hogg, E.H., Girardin, M.P., Lakusta, T., Johnston, M., Mckenney, D.W., Pedlar, J.H., Stratton, T., Sturrock,

R.N., Thompson, I.D., Trofymow, J.A., Venier, L.A., 2013. Anticipating the consequences of climate change for Canada's boreal forest ecosystems 1. Environ. Rev. 21, 322–365.
Roberts, D., Cooper, S., 1989. Concepts and techniques of vegetation mapping. In: Fergusson, D., Morgan, P., Johnsson, F.D. (Eds.), Land Classifications Based on Vegetation: Applications for Resource Management. USDA Forest Service, Ogden, UT, pp. 90–96.
Roy, D.P., Ju, J., Kline, K., Scaramuzza, P.L., Kovalskyy, V., Hansen, M., Loveland, T.R., Vermote, E., Zhang, C., 2010. Web-enabled Landsat Data (WELD): Landsat ETM+ composited mosaics of the conterminous United States. Remote Sens. Environ. 114, 35–49. https://doi.org/10.1016/j.rse.2009.08.011.
Sexton, J.O., Noojipady, P., Anand, A., Song, X.P., McMahon, S., Huang, C., Feng, M., Channan, S., Townshend, J.R., 2015. A model for the propagation of uncertainty from continuous estimates of tree cover to categorical forest cover and change. Remote Sens. Environ. 156, 418–425. https://doi.org/10.1016/j.rse.2014.08.038.
Sirois, L., Payette, S., 1989. Postfire black spruce establishment in subarctic and boreal Quebec. Can. J. For. Res. 19, 1571–1580. https://doi.org/10.1139/x89-239.
Song, C., Woodcock, C.E., Seto, K.C., Pax-Lenney, M., Macomber, S.A., 2001. Classification and change detection using Landsat TM data: when and how to correct atmospheric effects? Remote Sens. Environ. 75, 230–244. https://doi.org/10.1016/S0034-4257(00)00169-3.
Stinson, G., Kurz, W.A., Smyth, C.E., Neilson, E.T., Dymond, C.C., Metsaranta, J.M., Boisvenue, C., Rampley, G.J., Li, Q., White, T.M., Blain, D., 2011. An inventory-based analysis of Canada's managed forest carbon dynamics, 1990 to 2008. Glob. Chang. Biol. 17, 2227–2244. https://doi.org/10.1111/j.1365-2486.2010.02369.x.
Stocks, B.J., Mason, J.A., Todd, J.B., Bosch, E.M., Wotton, B.M., Amiro, B.D., Flannigan, M.D., Hirsch, K.G., Logan, K.A., Martell, D.L., Skinner, W.R., 2002. Large forest fires in Canada, 1959–1997. J. Geophys. Res. 108. https://doi.org/10.1029/2001JD000484.
Tachikawa, T., Kaku, M., Iwasaki, A., Gesch, D.B., Oimoen, M.J., Zhang, Z., Danielson, J.J., Krieger, T., Curtis, B., Haase, J., Abrams, M., 2011. ASTER Global Digital Elevation Model Version 2-summary of Validation Results.
Tompalski, P., Coops, N.C., White, J.C., Wulder, M.A., 2015. Enriching ALS-derived area-based estimates of volume through tree-level downscaling. Forests 6, 2608–2630. https://doi.org/10.3390/f6082608.
Tomppo, E.O., Gagliano, C., De Natale, F., Katila, M., McRoberts, R.E., 2009. Predicting categorical forest variables using an improved k-Nearest Neighbour estimator and Landsat imagery. Remote Sens. Environ. 113, 500–517. https://doi.org/10.1016/j.rse.2008.05.021.
Ung, C.-H., Bernier, P., Guo, X.-J., 2008. Canadian national biomass equations: new parameter estimates that include British Columbia data. Can. J. For. Res. 38, 1123–1132. https://doi.org/10.1139/X07-224.
Varhola, A., Coops, N.C., 2013. Estimation of watershed-level distributed forest structure metrics relevant to hydrologic modeling using LiDAR and Landsat. J. Hydrol. 487, 70–86. https://doi.org/10.1016/j.jhydrol.2013.02.032.
Varhola, A., Coops, N.C., Bater, C.W., Teti, P., Boon, S., Weiler, M., 2010. The influence of ground- and lidar-derived forest structure metrics on snow accumulation and ablation in disturbed forests. Can. J. For. Res. 40, 812–821. https://doi.org/10.1139/X10-008.
Vermote, E., Justice, C., Claverie, M., Franch, B., 2016. Preliminary analysis of the performance of the Landsat 8/OLI land surface reflectance product. Remote Sens. Environ. 185, 46–56. https://doi.org/10.1016/j.rse.2016.04.008.
Vogeler, J.C., Braaten, J.D., Slesak, R.A., Falkowski, M.J., 2018. Extracting the full value of the Landsat archive: inter-sensor harmonization for the mapping of Minnesota forest canopy cover (1973–2015). Remote Sens. Environ. 209, 363–374. https://doi.org/10.1016/j.rse.2018.02.046.
Wayson, C.A., Johnson, K.D., Cole, J.A., Olguín, M.I., Carrillo, O.I., Birdsey, R.A., 2015. Estimating uncertainty of allometric biomass equations with incomplete fit error information using a pseudo-data approach: methods. Ann. For. Sci. 72, 825–834. https://doi.org/10.1007/s13595-014-0436-7.
White, J.C., Wulder, M.A., 2014. The Landsat observation record of Canada: 1972–2012. Can. J. Remote Sens. 39, 455–467.
White, J.C., Wulder, M.A., Hobart, G.W., Luther, J.E., Hermosilla, T., Griffiths, P., Coops, N.C., Hall, R.J., Hostert, P., Dyk, A., Guindon, L., 2014. Pixel-based image compositing for large-area dense time series applications and science. Can. J. Remote Sens. 40, 192–212. https://doi.org/10.1080/07038992.2014.945827.
White, J.C., Wulder, M.A., Hermosilla, T., Coops, N.C., Hobart, G.W., 2017. A nationwide annual characterization of 25 years of forest disturbance and recovery for Canada using Landsat time series. Remote Sens. Environ. 194, 303–321. https://doi.org/10.1016/j.rse.2017.03.035.
Woodcock, C.E., Allen, R., Anderson, M., Belward, A., Bindschadler, R., Cohen, W., Gao, F., Goward, S.N., Helder, D.L., Helmer, E.H., Nemani, R.R., Oreopoulos, L., Schott, J., Thenkabail, P.S., Vermonte, E., Vogelmann, J.E., Wulder, M.A., Wynne, R.H., 2008. Free access to Landsat imagery. Science 320, 1011. https://doi.org/10.1126/science.320.5879.1011a. (80-.).
Wulder, M.A., Seemann, D., 2003. Forest inventory height update through the integration of lidar data with segmented Landsat imagery. Can. J. Remote Sens. 29, 536–543. https://doi.org/10.5589/m03-032.
Wulder, M.A., Campbell, C., White, J.C., Flannigan, M., Campbell, I.D., 2007. National circumstances in the international circumboreal community. For. Chron. 83, 539–556.
Wulder, M.A., White, J.C., Cranny, M.M., Hall, R.J., Luther, J.E., Beaudoin, A., Goodenough, D.G., Dechka, J.A., 2008a. Monitoring Canada's forests. Part 1: completion of the EOSD land cover project. Can. J. Remote Sens. 34, 549–562.
Wulder, M.A., White, J.C., Goward, S.N., Masek, J.G., Irons, J.R., Herold, M., Cohen, W.B., Loveland, T.R., Woodcock, C.E., 2008b. Landsat continuity: issues and opportunities for land cover monitoring. Remote Sens. Environ. 112, 955–969. https://doi.org/10.1016/j.rse.2007.07.004.
Wulder, M.A., Masek, J.G., Cohen, W.B., Loveland, T.R., Woodcock, C.E., 2012a. Opening the archive: how free data has enabled the science and monitoring promise of Landsat. Remote Sens. Environ. 122, 2–10. https://doi.org/10.1016/j.rse.2012.01.010.
Wulder, M.A., White, J.C., Bater, C.W., Coops, N.C., Hopkinson, C., Chen, G., 2012b. Lidar plots—a new large-area data collection option: context, concepts, and case study. Can. J. Remote Sens. 38, 600–618. https://doi.org/10.5589/m12-049.
Wulder, M.A., White, J.C., Nelson, R.F., Næsset, E., Ørka, H.O., Coops, N.C., Hilker, T., Bater, C.W., Gobakken, T., 2012c. Lidar sampling for large-area forest characterization: a review. Remote Sens. Environ. 121, 196–209. https://doi.org/10.1016/j.rse.2012.02.001.
Wulder, M.A., Coops, N.C., Roy, D.P., White, J.C., Hermosilla, T., 2018. Land cover 2.0. Int. J. Remote Sens. 39, 4254–4284. https://doi.org/10.1080/01431161.2018.1452075.
Zald, H.S.J., Ohmann, J.L., Roberts, H.M., Gregory, M.J., Henderson, E.B., McGaughey, R.J., Braaten, J., 2014. Influence of lidar, Landsat imagery, disturbance history, plot location accuracy, and plot size on accuracy of imputation maps of forest composition and structure. Remote Sens. Environ. 143, 26–38. https://doi.org/10.1016/j.rse.2013.12.013.
Zald, H.S.J., Wulder, M.A., White, J.C., Hilker, T., Hermosilla, T., Hobart, G.W., Coops, N.C., 2016. Integrating Landsat pixel composites and change metrics with lidar plots to predictively map forest structure and aboveground biomass in Saskatchewan, Canada. Remote Sens. Environ. 176, 188–201. https://doi.org/10.1016/j.rse.2016.01.015.
Zhu, Z., 2017. Change detection using Landsat time series: a review of frequencies, preprocessing, algorithms, and applications. ISPRS J. Photogramm. Remote Sens. 130, 370–384. https://doi.org/10.1016/j.isprsjprs.2017.06.013.
Zhu, X., Liu, D., 2015. Improving forest aboveground biomass estimation using seasonal Landsat NDVI time-series. ISPRS J. Photogramm. Remote Sens. 102, 222–231. https://doi.org/10.1016/j.isprsjprs.2014.08.014.